



**MACQUARIE**  
University  
SYDNEY • AUSTRALIA

# **Microstructural evidence of melt-present deformation and its effect on zircon modification**

---

**Masters of Research Thesis**

**Benjamin Alsop**

**10/11/2018**



**Department of Earth & Planetary Sciences in The Faculty of Science and Engineering,  
Macquarie University, North Ryde, Australia**

## Table of Contents

Statement of originality: .....	i
Acknowledgments.....	ii
Abstract.....	iii
Introduction .....	1
Recognising the former presence of melt .....	4
Zircons.....	5
Regional Geology .....	6
.....	9
Garnet reaction zone Interpretations.....	9
Methods.....	11
Fieldwork and Sample Collection.....	11
Petrography .....	11
Sample preparation .....	11
Backscatter electron imaging.....	11
Micro-energy-dispersive X-ray fluorescence microscopy ( $\mu$ -EDXRF).....	11
Zircon Separation .....	11
Rock crushing and selective fragmentation (Selfrag).....	11
Zircon imaging using scanning electron microscope .....	12
Laser-ablation inductively-coupled plasma mass spectrometry (LA-ICP-MS) .....	12
U-Pb dating .....	12
Trace element analysis.....	13
Previously analysed samples.....	13
Results.....	13
Field Relationships .....	13
Petrology.....	15
Weakly modified two pyroxene – plagioclase gneiss – PV1701B – representative of rocks south of the steeply dipping high strain zone.....	16
Hornblende – clinozoisite gneiss + plagioclase – PV1703B and associated strongly modified GRZ – PV1704 – representative of intermediate strain rocks north of the high strain zone.....	18
Hornblende – clinozoisite $\pm$ plagioclase gneiss – PV1705B1 .....	21
Hornblende-clinozoisite gneiss – PV1708.....	23
Steeply dipping high strain zone – PV1702C1.....	25
Modification due to strain .....	27

Microstructures.....	28
Small ( $\leq 60^\circ$ ) dihedral angles of interstitial grains (plagioclase, ilmenite, rutile & clinozoisite)...	28
Veinlets and elongate interstitial grains (plagioclase, rutile, clinozoisite).....	28
Melt pseudomorphs.....	28
Cuspate grains.....	28
Symplectites.....	29
Zircon Analysis .....	32
U-Pb geochronology .....	32
Weakly modified two-pyroxene – plagioclase gneiss – PV1232 (Elliot, 2016) .....	32
Trondhjemitic dyke – PV1234D.....	36
Hornblende-clinozoisite-plagioclase gneiss – PV1703B.....	36
Hornblende-clinozoisite gneiss – PV1708.....	37
Metre-scale thrust shear zone – PV1336B.....	37
Steeply dipping high strain zone – PV1702C1.....	38
Cumulative Probability Plots.....	38
Trace Element Patterns.....	38
Discussion.....	42
Microstructural criteria for recognising the former presence of melt in and immediately surrounding high strain zones.....	42
Small ( $\leq 60^\circ$ ) dihedral angles of interstitial grains .....	43
Veinlets and elongate interstitial grains .....	44
Melt pseudomorphs.....	44
Cuspate grains.....	44
Symplectites.....	45
Petrology .....	45
Melt-present deformation effect on magmatic zircon .....	46
Magmatic origin of zircon .....	46
Melt – present deformation .....	47
Zircon data errors and variable interpretations .....	48
Conclusion.....	50
Reference list .....	51



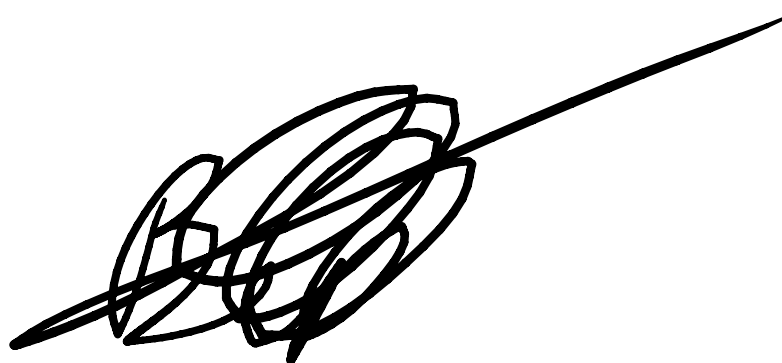
**Statement of originality:**

I certify that, to the best of my knowledge, the work presented herein is the original work of the author and has not been presented or published elsewhere. All published works and work carried out by persons other than the author presented here are appropriately referenced and due respect given to the participants. Further no part of this thesis has been presented, accepted or been published for the award or consideration of a higher degree or diploma at this or any other educational institution.

**Signed:**A small, stylized handwritten signature in black ink, consisting of several loops and a long horizontal stroke extending to the right.

Benjamin P Alsop

10/10/18

A large, bold, and highly stylized handwritten signature in black ink. It features multiple overlapping loops and a very long, straight horizontal line extending from the right side across the page.

## Acknowledgments

These last ten months have been nothing less than amazing. I am so grateful for this opportunity to extend my skills in every aspect of my life. The lessons that come from being the captain of my own personal project will stay with me for the remainder of my life and have played an enormous part in creating the person that I am today. In the week leading up to writing this section I found an old notebook I think it was from year 10, and in the back cover was a plan for after school. It went something like go to university (probably USYD) and do an engineering degree and end up working at an engineering firm. Well one of those predictions came true, I did go to university, but not the one I thought or in a discipline I had initially envisioned. But look at me almost eight years later submitting a Masters of Research Thesis, in a field that I can no longer see myself ever leaving, with a range of skills that I never knew existed.

Through this project I have been fortunate enough to visit some pretty amazing places and interacted with an array of amazing scientists and this is my attempt to thank them all.

First and foremost I would like to thank my principle supervisor Nathan Daczko, for sticking with me and being there throughout the thesis, door always open. I admire your incredible knowledge of all things metamorphic and structurally related, your big picture visualisation, memory and passion. I also am in awe of how you manage to provide just the right amount of help, to keep people's heads above water. Steve Foley and Tom Raimondo thank you for starting this journey with me by taking time away from your families to accompany Nathan and myself into the field and add your knowledge to the pool of information that I had available to me.

A big thank you to the GAU (Geochemical Analysis Unit) at Macquarie University for allowing me access to the facilities. In particular, many thanks to Tim Murphy and Yi-Jen Lai for your help analysing my samples. Thanks to Manal Bebbington for tirelessly making all of my thin sections for analysis. Thank you to Alex Stokes for access to the Optofab node of the Australian National Fabrication Facility, Macquarie University.

I am eternally grateful to my MRes cohort, Pete, Josh, Chris, Steph, Alice, Tom and Mike. Without you this year would not been nearly as fun as it was. All the lunches, dinners and random discussions about literally everything makes me smile looking back. I really hope that we remain in contact in the years to come and that we will always be friends.

## **Abstract**

The Earth's structure, chemistry, and the formation of mineral resources, require significant transfer of mass through the crust. Though pathways are identified such as dykes and shear zones, the recognition of these pathways can be improved and the effects of melt migration on zircon geochronology studied. This project examines a suite of variably strained outcrops associated with a m – scale shear zone in the Pembroke Granulite, Fiordland, New Zealand. This project shows an improved understanding of the signatures and processes associated with mass transfer by identifying five key microstructures indicative of the former presence of melt within intermediate to high strain zones in the Pembroke Granulite; 1) small dihedral angles of interstitial grains including plagioclase, clinozoisite, rutile and ilmenite; 2) veinlets/melt films pseudomorphed by plagioclase, clinozoisite and rutile; 3) melt pseudomorphs including biotite; 4) cusped grains; & 5) quartz – amphibole symplectites. Further development of this tool is the recognition on how melt-present deformation can modify zircons within a melt-fluxed system. This thesis proposes that microstructures indicative of the former presence of melt, and zircon modification, may be used as a tool for identifying rocks that formed during melt present deformation at variable strain intensities and potential shortfalls to interpretation.

## Introduction

Partial melting, melt migration and emplacement of melt within the Earth are central to the differentiation of the Earth's crust and allow for an understanding on how mass has moved through the crust over time. Current thinking about melt – rock reactions and fluid flow through the lower crust has changed in response to an increase in understanding of crustal dynamics. There is also a greater need to understand the significance of melt flux through the crust and how mass transfer works.

Melting is triggered by a rise in temperature above 630°C in most felsic, arkose and pelitic rocks. In mafic rocks, melting temperatures can be substantially higher based on the bulk composition, volatiles and confining pressure (Breton and Thompson, 1988; Sawyer, 1999). At temperatures above the solidus, unstable minerals start to melt. Two main melting styles that occur in the crust are; (1) Hydrous fluid - fluxed melting; and (2) dehydration melting. The former is a result of aqueous fluids fluxing through a high-temperature region of the crust (Weinberg and Hasalová, 2015). The latter, is a response to an increase in temperature and/or decompression in the absence of free aqueous fluid, with water being held in the reacting minerals (Clemens and Vielzeuf, 1987; Stuart et al., 2016).

Initially, melting occurs at triple junctions, where reactant minerals are in contact with each other, causing a melt pocket to form (Figure 1A). As heat increases, the melt volume increases and eventually coalesces to form an interconnected network (Figure 1B) (Sawyer, 1999). The amount of melt needed to form this network is not well defined, and depends on the bulk rock composition with Maaløe (1982) and Sawyer (1999) suggesting that there needs to be about 5% melt in a system before it becomes connected. A more recent study by Zhu et al. (2011) argues that at 2% melt in mantle peridotite there is interconnectedness, and the rock becomes permeable to migration. Maaløe (1982) suggests that deformation i.e. sheared flow, may decrease the threshold that is needed before a rock becomes permeable. In order for the melt to move there needs to be both a driving force to push the melt through the permeable rock and a site for the melt to migrate to (Sawyer, 1999).



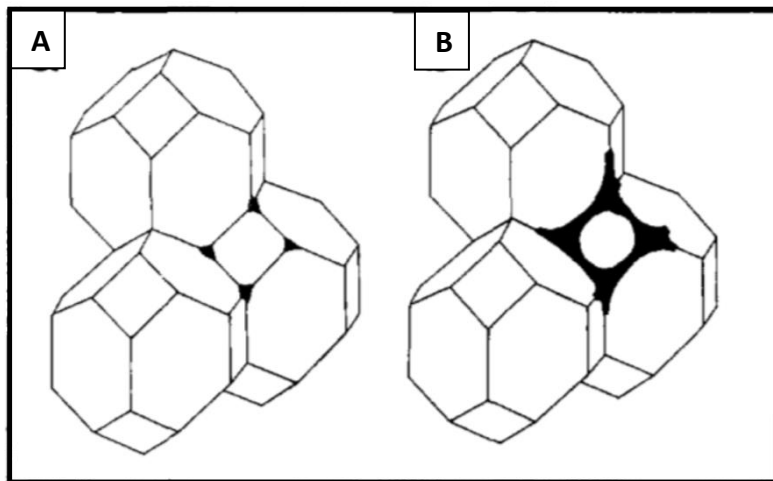


**Figure 1** - Diagram showing the change in melt geometry as the melt fraction increases (Sawyer, 1999)

- A. Start of melting; isolated pockets of melt located at grain triple junctions and corners
- B. Higher degree of melting causes the melt pockets to grow and coalesce forming an interconnected network within the rock

Methods for mass migration are greatly debated, with current thoughts suggesting mass travels as a low viscosity phase (as a melt or a supercritical fluid) and is highly dependent on crustal properties such as; pressure gradients, porosity, elasticity, yield strength, and fluid properties such as buoyancy and viscosity (Phipps Morgan and Holtzman, 2005; Sleep, 1988; Spence et al., 1987; Stuart et al., 2017). There are three main methods of significant mass transfer through the crust that occur with or without deformation. These occur in a brittle regime through dykes, ductile regimes at shear zones, and with/without deformation as diffuse porous flow. Dyking is an important mechanism for the transport of magmas in the Earth's crust and mantle (Spence et al., 1987; Weinberg, 1996) and has been studied extensively by the likes of Delaney and Pollard (1981); Delaney and Pollard (1982); Pollard (1973); Secor and Pollard (1975). The transport of magmas through dyking is driven by fluid overpressure and differential buoyancy of the magma relative to the country rock and its ability to fracture the rock (Spence et al., 1987). There exists a critical width that a dyke needs to be in order to facilitate the movement of magma without it freezing. The critical width required for felsic dykes to rise without freezing was estimated to be from a few metres to a few tens of metres. Dykes with widths below this critical point will take indefinitely long to grow and propagate, thus the magma that is traveling within the dyke will freeze, hindering melt migration (Weinberg, 1996). The self-propagating hydro-fracturing model of magma migration, proposes that small melt filled fractures, are able to propagate and coalesce, eventually draining into larger crustal scale features (Brown, 2010). These large scale features then propagate themselves as brittle cracks up through the crust, thus draining the source and transporting the melt to its final destination (Brown, 2010). Although this is a popular model, it does not leave much evidence behind for melt movement, meaning it is hard to distinguish as a viable method of melt movement (Brown, 2004; Brown, 2010). Ductile fracturing is a newer

method of melt migration and avoids the issues inherent in the self-propagating hydro-fracture method, which is supported by observations from residual granulites and migmatites. This model suggests that at depths below the brittle to ductile transition, thermally activated flow processes will lead to extensive inelastic deformation at the fracture tip (Brown, 2004; Brown, 2010).

Shear zones within the crust acts as conduits for the migration of fluids. There are many examples of shear zones recording mineralogical changes (Beach and Fyfe, 1972), that indicate they are zones for mass fluid movement. This is due to an inverted thermal gradient or up-temperature fluid flow (Beach and Fyfe, 1972; Cartwright and Barnicoat, 2003). This type of fluid flow can occur in several tectonic environments; 1) large-scale thrusting of hotter, dry rocks up over colder wetter rocks, where fluid flows from the footwall into the hanging wall which will be up temperature as an inverted thermal gradient (Beach and Fyfe, 1972; Cartwright and Barnicoat, 2003); 2) Fluid convection around cooling igneous plutons; 3) Topographical-driven fluid flow close to recharge areas; and, 4) Seismic pumping which is able to pump surface fluids down into the crust in ductile regimes (Cartwright and Barnicoat, 2003). Fluid flow in shear zones are not well defined, with varying models in the literature (Cartwright and Barnicoat, 2003). Two main methods are thought to be responsible for this migration: (1) Small dihedral angles that allows interconnectedness along grain boundaries (Figure 2A), or (2) Figure 2B shows that the fluid forms a number of discrete packages that is able to travel through the rock as it is deformed (Cartwright and Barnicoat, 2003).

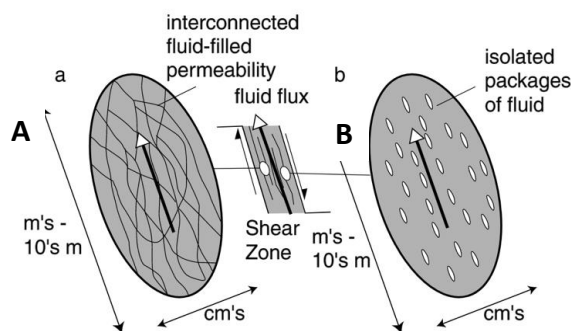


**Figure 2** – Alternate models of how fluid flows through shear zones (Cartwright and Barnicoat, 2003).

- A. The fluid forms an interconnected network around grain boundaries
- B. The fluid forms a number of discrete packages that is able to travel through the rock as it is deformed

Diffuse porous flow is a mechanism by which melt migrates from its source, runs along grain boundaries through overlying units. As fluid travels along grain boundaries, melt is disseminated in small pockets at grain boundaries and triple junctions (Stuart et al., 2016). For this to occur diffuse porous flow requires a solid framework, which breaks down at around 25% partial melting. Low dihedral angles ( $<60^\circ$ ) allows melt to wet grain boundaries, and at  $\sim 2\%$  partial melt an interconnected network of channels forms; helping facilitate the flow of melt through a solid rock

(Stuart et al., 2016; Zhu et al., 2011). Higher water content in a melt is shown to decrease the dihedral angles and increase the rocks ability to be connected (Stuart et al., 2016).

Diffuse porous flow occurs in an open system, thus is supplemented by melt-rock reactions (Stuart et al., 2016). Melt-rock reactions occur between solid host rock and migrating melt, that causes microstructural, and chemical changes, which can identify the former presence of melt, melt pathways, and estimation of melt compositions (Hasalová et al., 2008). Although deformation is not necessary for diffuse porous flow, there is generally a small viscosity difference between the host rock and melt moving, which assists deformation through shear zones (Stuart et al., 2016). The Identification diffuse porous flow as a migration method for melt is most likely hindered by comparatively complex melt-rock reactions, and overprinting of melt-flow textures driven by metamorphic and/or tectonic events during exhumation.

### **Recognising the former presence of melt**

The former presence of melt and the melt – rock interactions with different assemblages at outcrop scale can often be used to identify a sequence of melt-related events, providing insights into regional geological events. While some outcrops may indicate melt flux easily in the form of dykes or sills, some outcrops do not demonstrate the former presence of melt without further microscale investigation. Sawyer (1999) & Vernon (2011) list reliable criteria that can be used in the recognition of the former presence of melt, including: 1) three mineral aggregates of quartz, K – feldspar and sodic plagioclase in veins, 2) euhedral crystals of feldspar, or peritectic minerals lining felsic protoleucosomes, 3) - simple twinning of feldspar, 4) low dihedral angles ( $<60^\circ$ ) between grains inferred to have pseudomorphed former melt and 2 other grains, 4) aligned, euhedral feldspars, 6) inclusion free overgrowths of euhedral feldspar, 7) cusped grains of quartz, K-feldspar or sodic plagioclase, 8) veinlets of inferred former melt, 9) - veinlets of plagioclase that is more sodic than plagioclase grains in the adjacent rock, 10) – biotite being pseudomorphed by feldspar, 11) - plagioclase with oscillatory zoning, 12) microgranophyric intergrowths of quartz and alkali feldspar in patches or veins between primary grains, 13) symplectic replacement aggregates, 14) melanosome patches and layers, from which leucosome has been extracted, 15) inclusion free euhedral overgrowths of feldspar onto residual grains of feldspar with abundant inclusion. These recognition criteria can be applied to rocks that have veins and dykes as well as rocks that have been fluxed by melt at the grain scale. As with all geological systems, there is a degree of variability that means that only a few of the identification criteria may be present in some

examples. Care is also needed as some of the criteria can be the result of a melt-absent deformation, and give a false reading to the former presence of melt.

## **Zircons**

Zircons can be extremely variable in their external morphology and internal crystal structure. These structures reflect the geological history of the mineral, particularly episodes of magmatic or metamorphic (re)crystallization, and fluid alteration (Corfu et al., 2003). Much of the geological usefulness of zircons comes from its suitability as a geochronometer based on the decay of U - Pb. In addition, zircons contain Hf which is used to determine the HF isotopic compositions of grains and REE and other trace element abundances can also record useful information for inferring the history of the host rock and potentially the parental rock from which the zircon has originated prior to magmatic and metamorphic processes (Corfu et al., 2003; Langone and Tiepolo, 2015).

One of the major advantages of zircons is the ability to survive magmatic and metamorphic processes that destroy other common minerals. However this is also a disadvantage due to the fact that zircons have a high closure temperature meaning that they can fail to date tectonic processes at temperatures below the amphibolite facies (Langone and Tiepolo, 2015; Tulloch et al., 2011). When a zircon (de)forming event occurs it may be preserved as a distinct structural texture on a pre-existing zircon grain. As a result, it is quite common for a zircon to consist of distinct segments, each preserving a particular period of zircon alteration (Corfu et al., 2003; Wu and Zheng, 2004). This internal structure is impossible to identify with conventional binocular microscope techniques. Cathodoluminescence (CL) is a technique that is able to image the internal structure by bombarding the zircon with electrons. Based on the trace element composition of the zircon, the internal structure of the grain will be revealed. Potentially the most important task in zircon interpretation is the proper assignment of particular zircon domains or grains to a specific event in its history. This can be a relatively simple task where a proper understanding of the geological setting combined with logical deduction and scientific reasoning lead to a straightforward interpretation (Corfu et al., 2003).

The internal zoning of the zircons reflects the compositional variation of Zr and Si as well as variations in Hf, P, Y, the REE, U and Th. This variation leads to some interesting and complex structures within the grains (Corfu et al., 2003; Wu and Zheng, 2004). One of the most typical features of magmatic zircons is the presence of well-preserved oscillatory zoning, narrow bands of strong CL contrasts, indicating a magmatic alteration period (Wu and Zheng, 2004). This is possibly

due to the temperatures at which the melt was crystallising, as temperature is able to influence diffusion rates of trace elements. The second pattern that is observed in zircons are broader diffuse patterns. These show that the zircon formed under metamorphic conditions, be it temperature, pressure or fluid related (Wu and Zheng, 2004). The patterns commonly observed in this process tend to be sector zoning, patchy zoning, weak zoning, flow zoning and no zoning (Wu and Zheng, 2004). By analysing the REE compositions as well as absolute dating it is possible to gather a more geologically meaningful interpretation.

There are several potential pitfalls to using and interpreting zircons these include; 1) sampling bias – using a larger proportion of the LA-ICP-MS signal in interpretation will give a smaller error range but may mean the interpretation is geologically impossible, while using a smaller proportion of the signal may make for a more geologically meaningful result but the error may also increase, 2) Zircon modification and disturbance – due to zircons being able to record magmatic and metamorphic events, later modification may overprint and obscure the true history of the zircon grains.

## **Significance**

The generation and migration of melt is, one of the key processes that aid in crustal-scale mass transfer. Thus, understanding the possible modes of melt migration in the crust is of fundamental importance to Earth Science. It will further our understanding of how crustal-scale chemistry and matter flows within the crust, and is intrinsically linked to the formation of many styles of ore deposit at the Earth scale. Migrating melt must leave its mark in the host rock causing permanent modifications in terms of chemistry, microstructure and mineral assemblage. This thesis will help establish a set of chemical and physical criteria enabling the recognition of melt-rock interactions having once occurred in a region of interest, particularly in poorly exposed and over printed terrains common in Australia, by first establishing the criteria in exceptionally well exposed rocks and transferring that knowledge to small outcrops and hand samples from elsewhere.

## **Regional Geology**

New Zealand's South Island is made up of three major domains; the Eastern and Western Province is comprised of volcanic and sedimentary terranes, separated by the Median Batholith (Bradshaw, 1990; Daczko et al., 2001a; Hollis et al., 2003; Landis and Coombs, 1967; Mortimer et al., 1999; Stevenson et al., 2005; Stuart et al., 2017). This Batholith represents a 250 My record of arc-related magmatism that changed from calc-alkaline magmatism around 130 – 125 Ma to higher Sr

magmatism that occurred around 126 – 115 Ma (Daczko et al., 2001a; Daczko and Halpin, 2009; Stuart et al., 2016; Stuart et al., 2017). The Western Fiordland Orthogneiss (WFO) is the dominant expression of high Sr magmatism in the region, which shows variable degrees of deformation from relict igneous to granoblastic gneissose textures, and localized shear zones (Daczko and Halpin, 2009). Slightly older, the Arthur River Complex is comprised of dioritic gneiss, and gabbroic gneiss which outcrops as the Pembroke Granulite located within the in the Pembroke Valley, just north of Milford Sound, (Figure 3) (Daczko et al., 2001a).

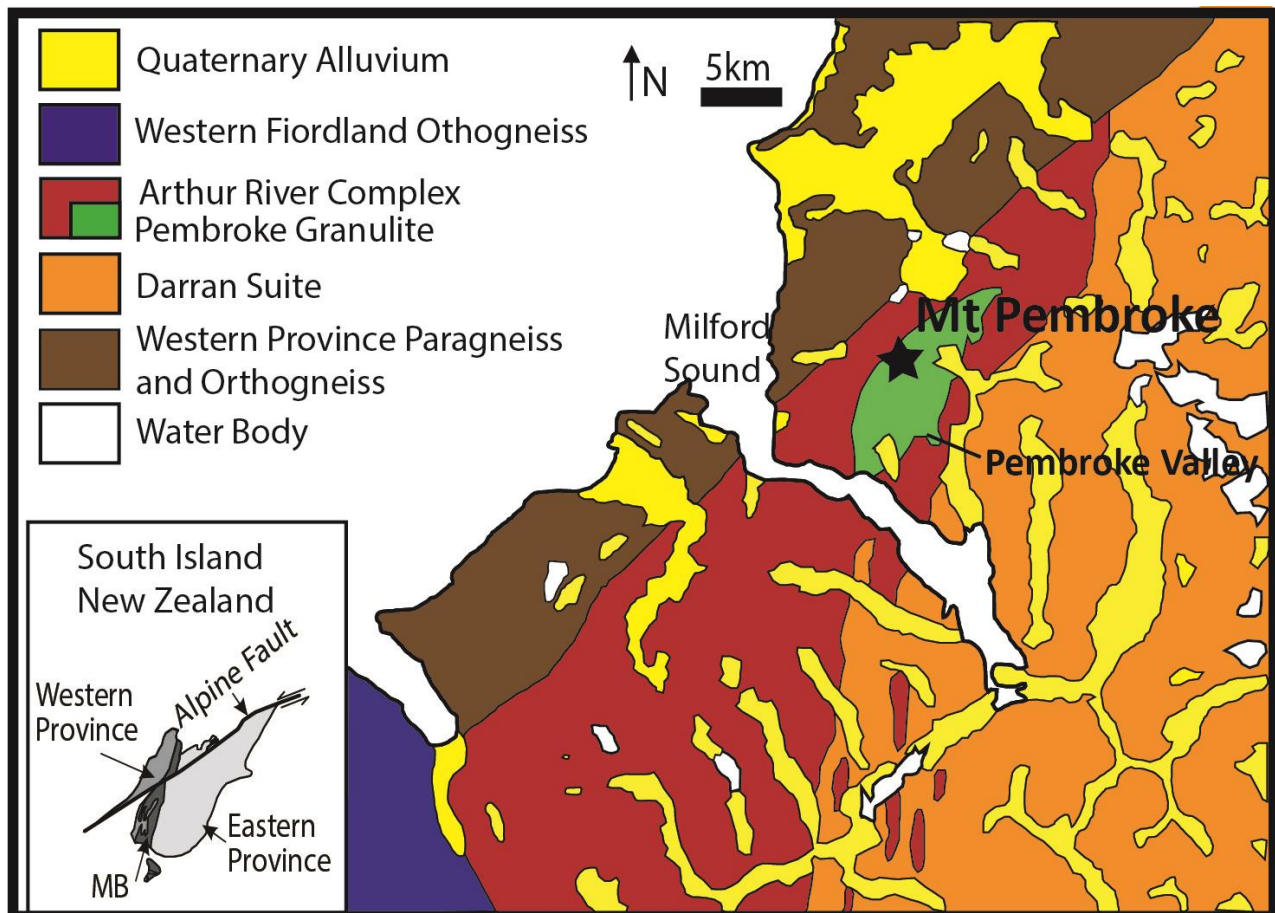


**Figure 3** - Geological map of Northern Fiordland, New Zealand, showing major lithological divisions and location of study area modified from (Daczko and Halpin, 2009; Stuart et al., 2016) .

The Pembroke Granulite lies in the western part of the Median Batholith and forms a low-strain zone that preserves lower crustal mineralogy and microstructures. It is a gabbroic gneiss that was emplaced from 139 – 129 Ma (Hollis et al., 2003) or 163 – 150 Ma (Stowell et al., 2010), making it a disputed region of the Median Batholith. Both these suggested ages of emplacement overlap with the ages suggested for the Darran Suite (Stuart et al., 2017). The Pembroke Granulite outcrops within the Pembroke Valley, where exposures spans 1 km long, 150 m wide, with a height of 220

m. The Pembroke Granulite is generally two-pyroxene-pargasite gabbroic gneiss with intermittent pods of dioritic compositions and ultrabasic granofels usually found within dioritic rocks as dark pods (Clarke et al., 2005; Daczko et al., 2001a; Stuart et al., 2017). Published data shows that the Pembroke Granulite has undergone several deformation and metamorphic events, with mineral assemblages indicating that peak metamorphic conditions were between 8 - 14 kbar and  $T > 750^{\circ}\text{C}$  (Daczko and Halpin, 2009; Stowell et al., 2014; Stowell et al., 2010; Stuart et al., 2016; Stuart et al., 2017).

Igneous assemblages are recrystallised due to D1 events that resulted in a pervasive S1 gneissic foliation, defined by enstatite, diopside, pargasite, plagioclase, and ilmenite, with P-T estimates varying from  $<6$  to  $<11$  kbar and  $650\text{--}850^{\circ}\text{C}$  (Daczko et al., 2001a; Daczko and Halpin, 2009; Stuart et al., 2016; Stuart et al., 2017). These S1 assemblages are partially hydrated to pargasite, quartz, clinozoisite and plagioclase post D1 during an episode of melt assisted diffuse porous melt flow under static conditions just above the solidus ( $630 - 710^{\circ}\text{C}$  and  $8.8 - 12.4$  kbar) and records partial hydration of the lower crust during the melt flux event (Stuart et al., 2016; Stuart et al., 2017). D2 involves sub-planar and steeply dipping plagioclase-rich dykes, that cut S1 in a distinctive rectilinear pattern (Daczko et al., 2001a; Stuart et al., 2016). Neighbouring these dykes at a scale of 1 - 10 cm the S1 minerals have been replaced by garnet granulite defined by an assemblage of garnet, plagioclase and clinopyroxene, that outcrops as a distinctive pink alteration band termed garnet reaction zones (GRZ) (Figure 4). These assemblages are thought to be due to a trondhjemitic melt that has scavenged volatiles from the host gabbroic gneiss at P - T conditions around 12 - 16 kbar and  $720 - 890^{\circ}\text{C}$  (Clarke et al., 2005; Daczko et al., 2001a; Stuart et al., 2016). The gabbroic gneiss, S1 and the GRZ features are variably deformed by D3, which involves east-striking, steeply dipping, narrow cm - m wide shear zones that preserve evidence for dominantly sinistral displacement (Daczko et al., 2001a); these were active at P-T conditions 14 kbar and  $676^{\circ}\text{C}$  (Figure 5) (Daczko et al., 2001a; Stuart et al., 2016). A steeply dipping D<sub>3</sub> shear zone was mapped in detail for this study and is compared to a m - scale thrust shear zone analysed by Daczko et al. (2001b) and Elliot (2016).

The Pembroke Granulite provides an exceptional field area to study the mechanisms of complex melt-rock interactions due to mass transfer, as it has been exhumed from depths of 45km with little tectonic and metamorphic overprinting, thus providing a snapshot of the earth's deep crust.

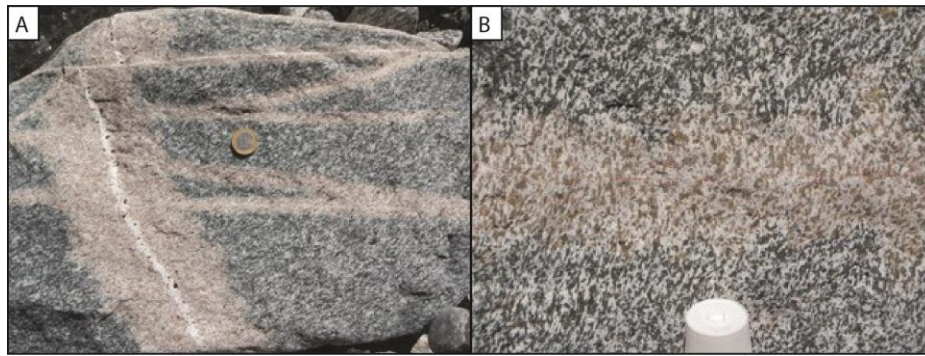


**Figure 4** – Garnet Reaction Zone -Thin dykes and localized development of GRZ textures in irregular-shaped patches. These GRZ are typically 1-10 cm wide with some GRZ lacking a felsic dyke due to their collapse once melt has passed through.

- A. GRZ showing centralised plagioclase dyke
- B. GRZ with collapsed plagioclase dyke

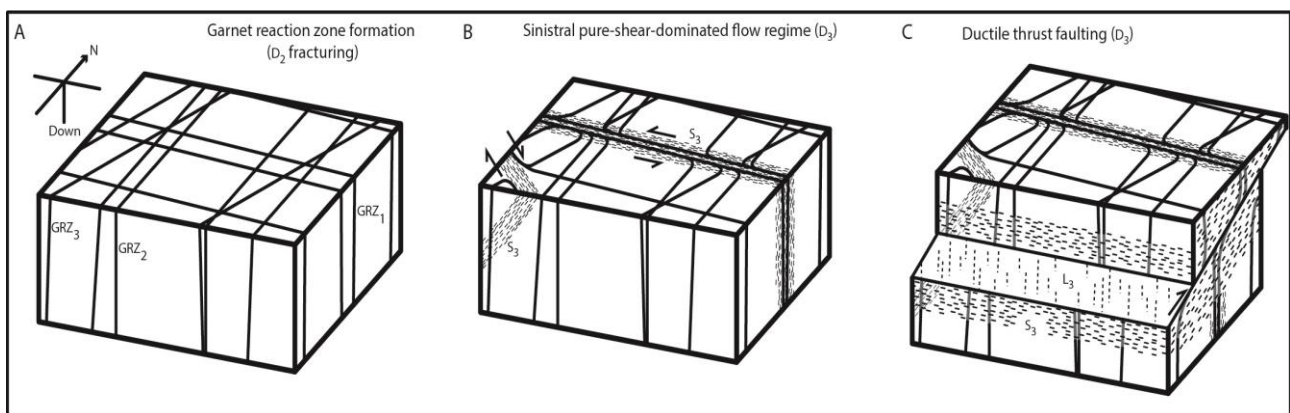


**Figure 5** - Block diagram of the key deformation events within the Pembroke Granulite. D1 resulted in a pervasive S1 gneissic foliation; D2 involves anorthositic dykes and fractures cutting S1 in a rectilinear pattern, D3 involves east-striking, steeply dipping & thrust, narrow cm-m shear zones which show sinistral displacement. Altered from Clarke et al. (2000); Daczko et al. (2001b)

## Garnet reaction zone Interpretations

The most disputed area of research in the Pembroke Granulite studies are the Garnet Reaction Zones (GRZ). The GRZ are recrystallised and spatially restricted garnet granulite that are adjacent to narrow anorthositic dykes that cut hornblende-bearing orthogneiss (Clarke et al., 2005). There are currently two main views relating to the interpretation of these GRZ; one put forward by Blattner (1976); Blattner (2005) and the other by Daczko et al. (2001a).

Blattner (1976); Blattner (2005) presents a metasomatic model that involves local migration of a carbonic-rich and sodic-rich dehydrating fluid to form the GRZ structures. Daczko et al. (2001a); suggest however, a trondhjemitic liquid, sourced from the partial melting of adjacent bodies of dioritic gneiss and its subsequent migration through the gabbroic gneiss, has gained its required H<sub>2</sub>O (mostly from hornblende) to induce the GRZ hosted by the gabbroic gneiss.



The main issues with the Blattner (1976) interpretation involving a carbonic fluid along pre-existing vein networks leading to the dehydration of the adjacent rocks are;

- 1) there is no confirmed source or sink for the CO<sub>2</sub> fluid (Clarke et al., 2005),
- 2) The termination of the GRZ at lithological boundaries of rocks that are mineralogically close to the GRZ host rock composition, especially since the dykes that are central to the GRZ continue across the lithological boundary.

If Blattner's interpretation were correct a special fluid would need to be present. This fluid would need to be capable of creating sharp boundaries, have a radiogenic signature close to that of the host rock, be capable of causing dehydration in one lithology but not a second and be capable of causing metre wide variation in mineralogy (Clarke et al., 2005). Given there is no physical evidence of this liquid, it can be argued that Blattner's interpretation is incorrect.

Also, there are issues with the interpretation by Daczko et al. (2001a), primarily originating from Blattner (2005). Blattner (2005) suggests that many of the GRZ contain no plagioclase-rich central films or veins that are expected to be the transport mechanism of the melt. Daczko and Halpin (2009) counter this by suggesting that the central dykes and veins narrowed and closed after melt had fluxed through the rock leaving the GRZ as a melt rock interaction texture and a marker, to the now closed, melt migration pathway (Figure 4B). This interpretation of an igneous melt flux is supported by Stuart et al. (2016) who suggested that instead of partially melting the adjacent body of dioritic gneiss, an external fluid is required to flux through the region in order for the hydration of the host rock to occur.

Stuart et al. (2016) go on to offer a new and more plausible interpretation; a model involving migration of an externally-derived melt which would result in changes to the bulk rock chemistry that would be directly related to the amount, and type of melt migrating through the rock. Chemical analysis was performed by Stuart et al. (2016) to test this interpretation, and they identified that the bulk rock compositions in the Pembroke Granulite are extraordinarily similar to the regions of high melt flux that occurred in certain regions of Pembroke Granulite. This implies that there was little to no melt stagnating and subsequent crystallization in the host rock, instead invoking a model of melt flux where most of the melt fraction passes through leaving little melt to crystallize in the solid host. This new interpretation involved using identification criteria to show the former presence of melt, rather than bulk rock chemistry.

## **Methods**

### **Fieldwork and Sample Collection**

Fieldwork was conducted in the Upper Pembroke Valley, located to the north of Milford Sound, and at the base of Mt Pembroke, New Zealand, between 8–9<sup>th</sup> December 2017. The area investigated is part of the Arthur River Complex and provides excellent exposure of lower crustal rocks exhumed from depths over 45km with minimal retrograde tectonic and metamorphic overprint.

### **Petrography**

#### **Sample preparation**

Samples were prepared at MQ Geoanalytical, Macquarie University. 22 samples were mounted to glass thin section slides and polished to ~30 microns thick, to perform imaging and chemical analysis on. Six samples (PV1701B, PV1702C1, PV1703, PV1704, PV1705B1 and PV1708) were chosen for more detailed analysis.

#### **Backscatter electron imaging**

Backscatter electron (BSE) images were used for characterisation of microstructure as well as mineral identification. The polished thin sections were carbon coated and imaged using a Hitachi tabletop TM4000 scanning electron microscope (SEM), at the Macquarie University node of the Australian National Fabrication Facility – OptoFab. Operating conditions were in a vacuum, at an accelerating voltage of 15 kV, a working distance of 8-10 mm, and a magnification of 40–400 times.

#### **Micro-energy-dispersive X-ray fluorescence microscopy ( $\mu$ -EDXRF)**

For  $\mu$ -EDXRF data acquisition, a Bruker M4 Tornado was used at MQ Geoanalytical, Macquarie University; all analyses were undertaken at 20 mbar vacuum. This system has an Rh X-ray tube with a Be side window and polycapillary optics giving an X-ray beam with a diameter of 25–30  $\mu$ m on the sample operating at 50kV and 600  $\mu$ A. The thin sections were scanned with a step size (pixel size) of 40  $\mu$ m and a dwell time of 25 ms per detector per pixel for a total of 50 ms per pixel dwell time. Each individual pixel was classified using the Advanced Mineral Identification and Characterization System (AMICS) proprietary software to attain mineral modes (area %).

### **Zircon Separation**

#### **Rock crushing and selective fragmentation (SelFrag)**

Three rock samples (steeply dipping high strain zone - PV1702C1, hornblende – clinozoisite gneiss + plagioclase - PV1703) and hornblende – clinozoisite gneiss - PV1708) of varying sizes and weights

were crushed (<3cm) under a hydraulic rock press. Samples were then disaggregated in the SelfFrag lab at MQ Geoanalytical, Macquarie University, with operating parameters set to 500 pulses, at a frequency of 5Hz, at 120kV, and an electrode gap of 10mm. This was performed until the samples became fully disaggregated.

Following disaggregation, all samples were sieved into >600 µm, 300–600 µm and <300 µm fractions. The <300 µm fraction was then panned to concentrate the heavy minerals which were further concentrated using standard magnetic (Frantz Magnetic Barrier Laboratory Separator) and heavy liquid (sodium polytungstate solution) mineral separation procedures. Zircon grains were hand-picked from the final concentrate under a binocular microscope with the aid of a UV lamp and mounted in epoxy and polished to expose a cross section of the grains.

#### Zircon imaging using scanning electron microscope

The mounted zircon grains (<300µm) were imaged and identified with a Scanning Electron Microscope (SEM), in CL imaging mode, at MQ Geoanalytical, Macquarie University. Zircon composition was checked using EDS prior to imaging. The imaging operating parameters were 25kV accelerating voltage, a working distance of 11.5–12 mm. Magnification varied by grain but most grains were imaged at about 150x magnification and once brightness and contrast settings were adjusted properly, external shape and internal structures such as zoning were imaged for each grain. Chemical composition was also checked to confirm each grain was zircon.

#### Laser-ablation inductively-coupled plasma mass spectrometry (LA-ICP-MS)

##### U-Pb dating

In situ U-Pb dating was performed on the imaged zircon grains following methods described by Jackson et al. (2004) and using a Photon Machines Excimer laser-ablation system with a beam wavelength of 193 nm attached to an Agilent 7700 series quadrupole ICP-MS at MQ Geoanalytical, Macquarie University.

Isotopes measured were  $^{204}\text{Pb}$ ,  $^{206}\text{Pb}$ ,  $^{207}\text{Pb}$ ,  $^{208}\text{Pb}$ ,  $^{232}\text{Th}$  and  $^{238}\text{U}$ . A laser pulse rate frequency of 5 Hz, burst count of 595 shots and fluence of 9.28 J/cm<sup>2</sup> was employed with a spot size of 40 µm used for all samples (PV1702C1, PV1703, PV1708). Ablated material was transferred from the sample by a mixture of Ar and He carrier gases. A single shot pre-ablation was performed before each analysis with 60 seconds of blank gas measurement and 120 seconds of acquisition. Reference zircon GJ-1 (Elhlou et al., 2006) was analysed twice at the beginning and end of each run of 12–14 unknowns as the bracketing standard for instrument calibration. Secondary internal

standards, 91500, Mud Tank and Temora, were also measured at the start and end of each run as an independent measure of instrument stability and data reproducibility. Data reduction and signal selection was performed using the GLITTER software package (<http://www.glitter-gemoc.com>). Due to the concordant nature of the zircons analysed, no common Pb correction was applied.

### Trace element analysis

In situ trace element analysis was undertaken on 73 grains for Si, P, Ti, Y, Zr, Nb, La, Ce, Pr, Nd, Sm, Eu, Gd, Dy, Ho, Er, Yb, Lu, Hf, Ta, Pb, Th and U. Operating conditions and equipment were as described for U-Pb dating, with NIST 610 glass measured as the external calibration standard and a spot size of 40  $\mu\text{m}$ . Secondary internal standards, GJ-1 and BCR-2 (Jochum et al., 2016), were measured at the start and end of each run as an independent measure of instrument stability and data reproducibility. The GLITTER software package was used to select homogenous sections of signal in order to avoid possible inclusions within the zircon. Trace element concentrations were then calibrated using Zr, assuming perfect stoichiometry (66 wt%) also with the GLITTER software package.

### Previously analysed samples

There are three additional samples that have been analysed in previous works that will be reported in this thesis; these are Two-pyroxene-pargasite gneiss (PV1232), trondhjemitic dyke (PV1234D) and m-scale thrust shear zone (PV1336B). These samples were prepared in the same way as described above. Analysis was carried out in the same operating conditions as the samples described above.

## Results

### Field Relationships

Rocks in the Pembroke Valley have recently been exposed due to retreat of the Pembroke Glacier. This study investigated hornblende-rich rocks that outcrop in the upper reaches of the valley. The samples described in this thesis are all modified versions of the well-studied Pembroke Granulite. The granulite comprises gabbroic gneiss (two-pyroxene–plagioclase  $\pm$  hornblende) that is cut by a spectacular grid of thin plagioclase-rich dykes with garnet reaction zones (Figure 6A, B). These assemblages are variably modified in the study area that is focused around a steeply dipping 2–4m wide high strain zone (Figure 7). Described in order of increasing strain, the examined rocks are: weakly modified two-pyroxene–plagioclase gneiss to the south of the steeply dipping high strain zone (low strain, Figure 6A,B), hornblende-clinzoisite gneiss to the north of the steeply dipping

high strain zone (moderate strain, Figure 6C,D) and a steeply dipping high strain zone comprising banded amphibolite (Figure 6E,F). Increasing strain is mapped by a change in angle between the GRZ. In the lower strain regions, the GRZ have a rectilinear outcrop pattern (Figure 6A) with dominant angles of 90° between the two main sets. As strain increases, the dominant angle between GRZ reduces to ~30–45° in the intermediate strain rocks (Figure 6B) and to <20° in the high strain rocks (Figure 6 (E,F), where the GRZ are difficult to distinguish).

The outcrop pattern of the Pembroke Valley field site (Figure 7A) is shown in a drone aerial view (Figure 7B). Ten sites were investigated (Figure 7B) for in situ samples to be taken back to Macquarie University for further investigation. The last site (red box in Figure 7B) was mapped in detail (2x1 m<sup>2</sup> grid), which was photographed using a camera mounted on a 3m pole and the photographs were stitched together to form a high-resolution image which was then hand mapped in further detail (Figure 7C). 3D interactive models of the Pembroke Valley field site and detailed grid map (Figure 7B & C) can be found at the following links respectively.

<https://mq.pedestal3d.xyz/viewer/?id=482&mode=normal>

<https://mq.pedestal3d.xyz/viewer/?id=481&mode=normal>

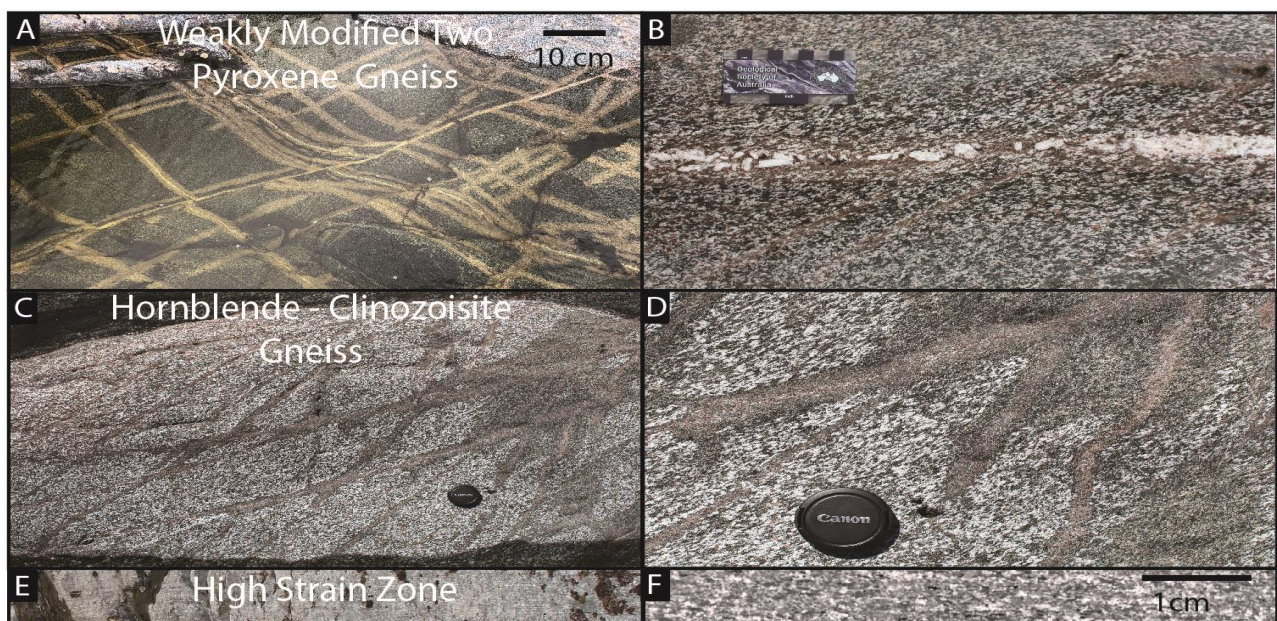


**Figure 6 – Field relationships of examined rocks**

- A. Weakly modified two pyroxene – plagioclase gneiss in the low strain zone – showing rectilinear GRZ outcrop patterns
- B. Close up of the GRZ in the weakly modified two pyroxene – gneiss
- C. Hornblende – clinzoisite gneiss in the moderate strain zones – showing GRZ at reduced angles to each other
- D. Close up of the outcrop pattern of the hornblende – clinzoisite gneiss
- E. Field relationship of the steeply dipping high strain zone
- F. Close up of the steeply dipping high strain zone



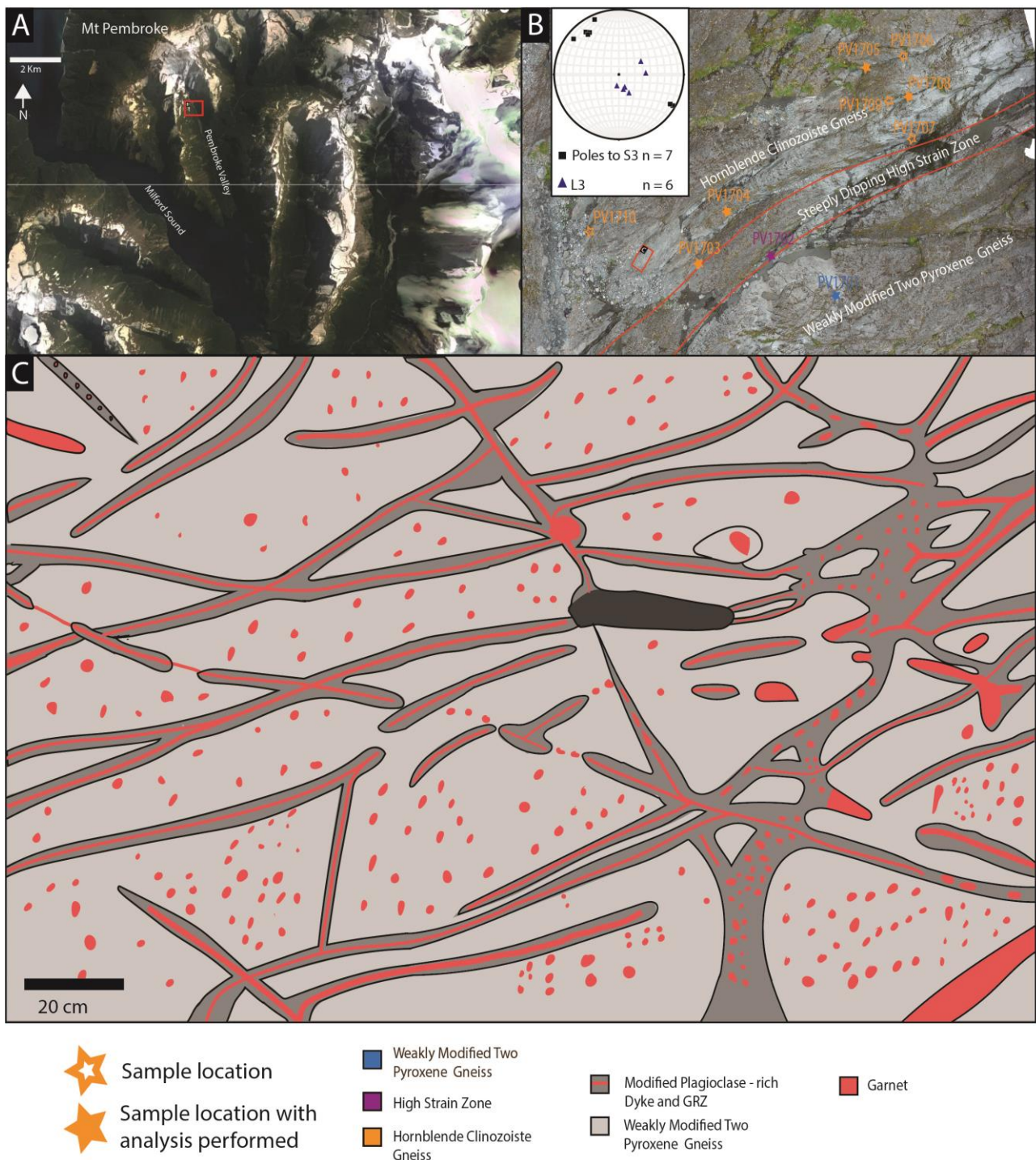


**Figure 7**

A – Overview map of the Pembroke valley in relation to Milford Sound and Milford village. The red box in the figure represents the field site.

B – Aerial map of Pembroke Valley, Fiordland, New Zealand, showing major sample locations, detailed field observation site (C) and major unit boundaries. Created using stitched drone photography- with stereonet of  $D_3$  elements ( $L_3$  and poles to  $S_3$ ) for the steeply dipping high strain zone

C – Grid map of hornblende – clinozoisite ± plagioclase gneiss – showing a close-up relationship between GRZ and surrounding host rock

## Petrology

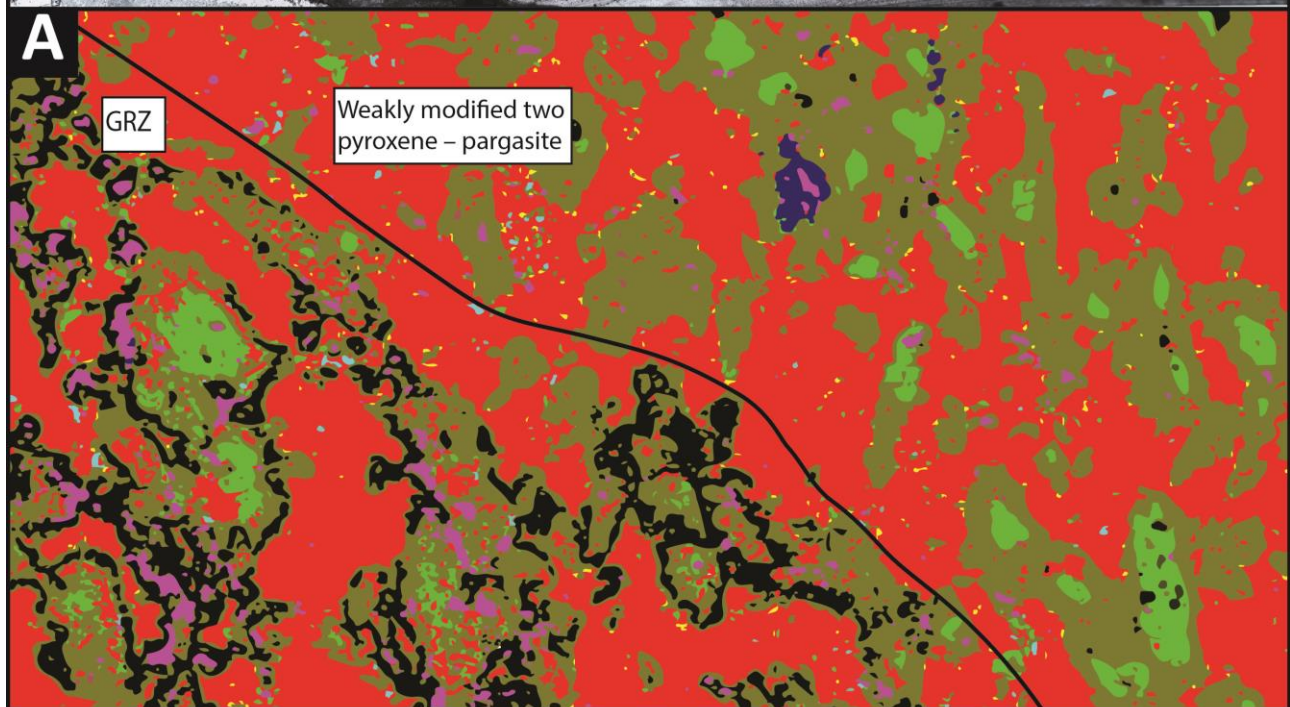
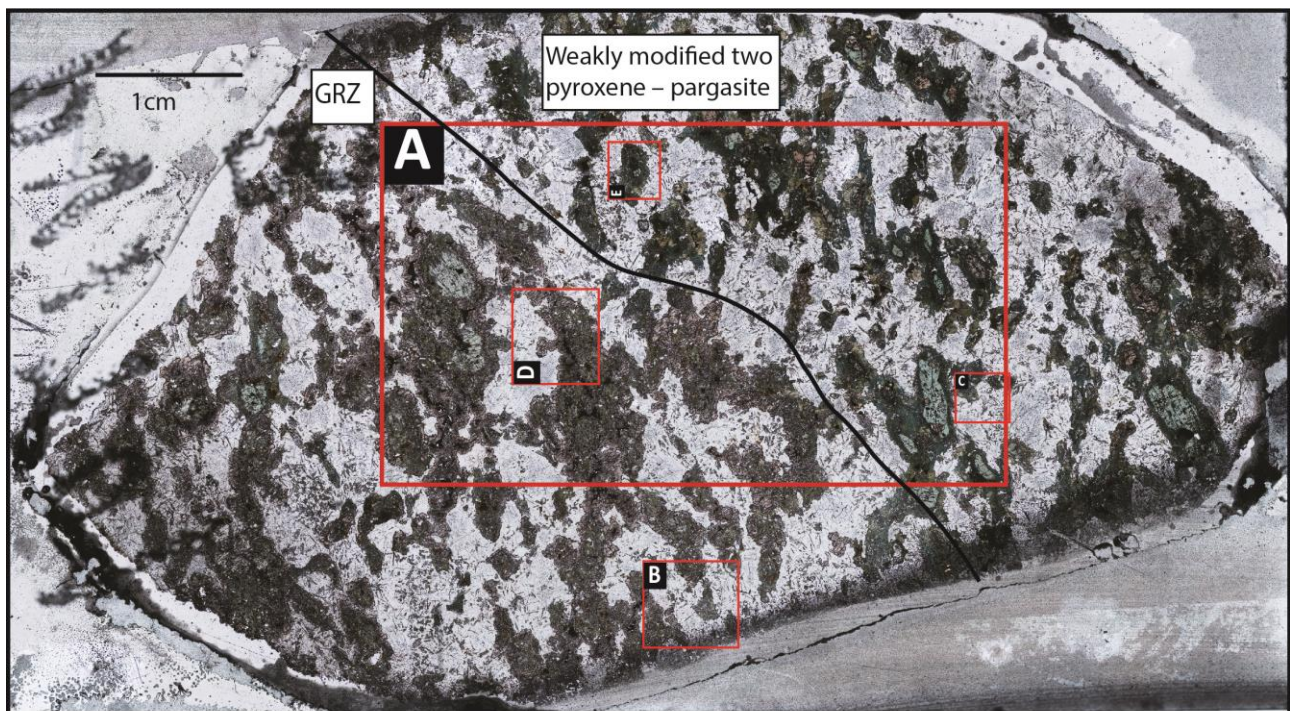
### Weakly modified two pyroxene – plagioclase gneiss – PV1701B – representative of rocks south of the steeply dipping high strain zone

The gabbroic gneiss with GRZ is well exposed throughout the valley and forms the majority of the rock found in the valley. It consists of elongate two-pyroxene-pargasite mafic clusters that define the gneissic foliation (S1) within a plagioclase-rich matrix (Daczko et al., 2001a). This unit also contains narrow (20–40mm wide) felsic (plagioclase-rich  $\pm$  garnet-quartz-K-feldspar) dykes that cut the gneissic fabric in a rectilinear pattern (Figure 6C). Either side of these felsic dykes are 10–20mm wide reaction zones, where the gabbroic gneiss is pseudomorphed by garnet granulite (GRZ). It is common for the garnet reaction zones to exist without an associated dyke structure.

There are two distinct domains to the representative low-strain sample (Figure 8). The GRZ domain is comprised of coarse grained (3–4 mm) amphibole (30.25%), variably sized plagioclase (1–10mm) (42.26%) and garnet (16.02%) that appears in coronate microstructures surrounding a complex symplectite of plagioclase and amphibole. At the centre of this symplectite is an inner grain of clinopyroxene (3.73%) (Figure 8D). Accessory minerals within the GRZ include: clinozoisite (0.32%), apatite (0.19%), rutile (1.49%), ilmenite (5.67%) and titanite (0.07%). These titanium bearing minerals appear to be associated with the garnet coronas and not randomly distributed throughout this half of the sample.

Within the garnet-poor domain of this sample, the two main minerals are amphibole and plagioclase which comprise 40.59% and 50.79% of the sample. Plagioclase grains display various deformation features such as tapered twinning and kink bands (Figure 8B,C). Accessory minerals include: clinopyroxene (3.32%) which form colourless, elongate crystals that are either euhedral, singular grains or exhibit a splayed texture when grouped, clinozoisite (0.18%) which appear as randomly orientated, fine grained crystals scattered throughout the sample, garnet (1.77%) which appear as larger individual crystals and in some regions demonstrates a corona texture (Figure 8E). Apatite (0.76%) which appears as larger grains and not distributed throughout the sample, rutile (0.53%), ilmenite (2.03%) and titanite (0.02%) are all randomly distributed throughout this half of the sample and do not appear to be associated with a singular mineral, like those in the GRZ domain.





PV1701B	Area %	
Mineral	Host	GRZ
Amphibole	40.59	30.25
Plagioclase	50.79	42.26
Clinozoisite	0.18	0.32
Garnet	2.77	16.02
Apatite	0.76	0.19
Biotite	0.00	0.00
Rutile	0.53	1.49
Ilmenite	2.03	5.67
Titanite	0.02	0.07
Quartz	0.00	0.00
Clinopyroxene	2.32	3.73
Other	0.00	0.00
Total	100.00	100.00

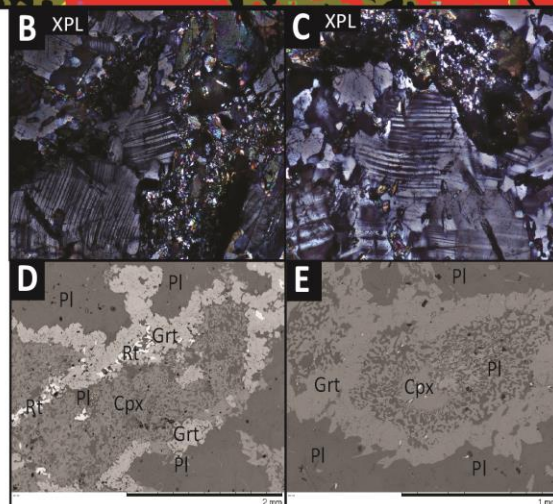




**Figure 8 – Weakly modified two pyroxene – plagioclase gneiss – PV1701B**

Modal percentages have been normalised to 100% for each domain to allow for direct comparison between samples

- A. u-XRF Mineral Map - the lower half of the sample is weakly modified GRZ domain while the upper half is weakly modified host domain. Yellow area's represent grain boundaries where the u-XRF cannot distinguish between amphibole and plagioclase - these regions have been divided evenly between the amphibole and plagioclase (in all samples)
- B. Photomicrograph of plagioclase demonstrating deformation features such as tapered twinning and kink bands
- C. Photomicrograph of plagioclase demonstrating deformation features such as tapered twinning and kink bands
- D. BSE image showing corona and symplectite textures within the GRZ
- E. BSE image showing corona and symplectite textures within the host two pyroxene – pargasite gneiss

**Hornblende – clinozoisite gneiss + plagioclase – PV1703B and associated strongly modified GRZ – PV1704 – representative of intermediate strain rocks north of the high strain zone**

North of the high strain zone in the field area, the two pyroxene–plagioclase gneiss and GRZ are moderately strained as demonstrated by reduced angles between the GRZ (Figure 6B). The granulite is modified to hornblende–clinozoisite + plagioclase gneiss (Figure 7B). Samples PV1703B and PV1704 come from different areas of this unit but have been combined in order to describe the relationship between a garnet-rich zone (mapped as a former GRZ) and garnet-poor zone (mapped as former two-pyroxene-pargasite gneiss, host domain). Figure 9 demonstrates this split between the two domains with the upper half of the sample being the garnet poor sample (PV1703) while the lower half is the a modified GRZ that demonstrates mm-wide banding (PV1704). Spatially, these samples are about 3–4 m apart, as shown in Figure 7B.

Within the GRZ domain of the sample, amphibole is found throughout. It is primarily coarse grained (2–4 mm) and is mostly anhedral with some euhedral grains (52.42%). Plagioclase grains are 2–3mm in size and comprise 15.06% of the sample. Garnets are only found in this portion of the sample, ranging in size from <1mm–4 mm and are generally found within the amphibole rich areas (15.69%) (Figure 9D). However, small garnets are scattered throughout the plagioclase-rich regions (Figure 9E). Clinozoisite is fine (0.1–1mm) to coarse grained (2–3mm) and shows internal zonation in some grains (7.67%). There is a rough orientation similar to that of the amphibole in the coarser more elongate grains. Clinozoisite is usually associated with plagioclase and apatite. It is usually anhedral in the plagioclase and elongate when found within the darker amphibole rich areas.

The remainder of the domain is made up of accessory rutile (1.00%), ilmenite (0.93%) titanite (4.31%), apatite (0.86%), quartz (1.05 %) and biotite (1.04%). Titanium-bearing minerals are found throughout the domain and are usually attached to the garnet mineral. Apatite is also a minor component of this domain, scattered randomly throughout with a variable grain size. Biotite typically demonstrates a euhedral crystal structure and ranges from 1–3 mm in size. Quartz is a very small component of this sample and is associated with plagioclase.

Within the garnet-poor domain (PV1703); amphibole (54.75%) is distributed throughout the sample and is generally coarse grained (2–5 mm). It is mostly anhedral, although, some grains do show an almost perfect cleavage pattern of 60/120. There is an apparent alignment through the amphibole across the sample. Plagioclase (31.24%) ranges in size from 1–3 mm and is scattered throughout the sample. Clinozoisite (7.70%) is fine (0.1–1mm) to coarse grained (2–3mm) and shows optical internal zonation in some grains. There is a rough orientation similar to that of the amphibole in the coarser, more elongate grains. The clinozoisite is usually associated with plagioclase and apatite.

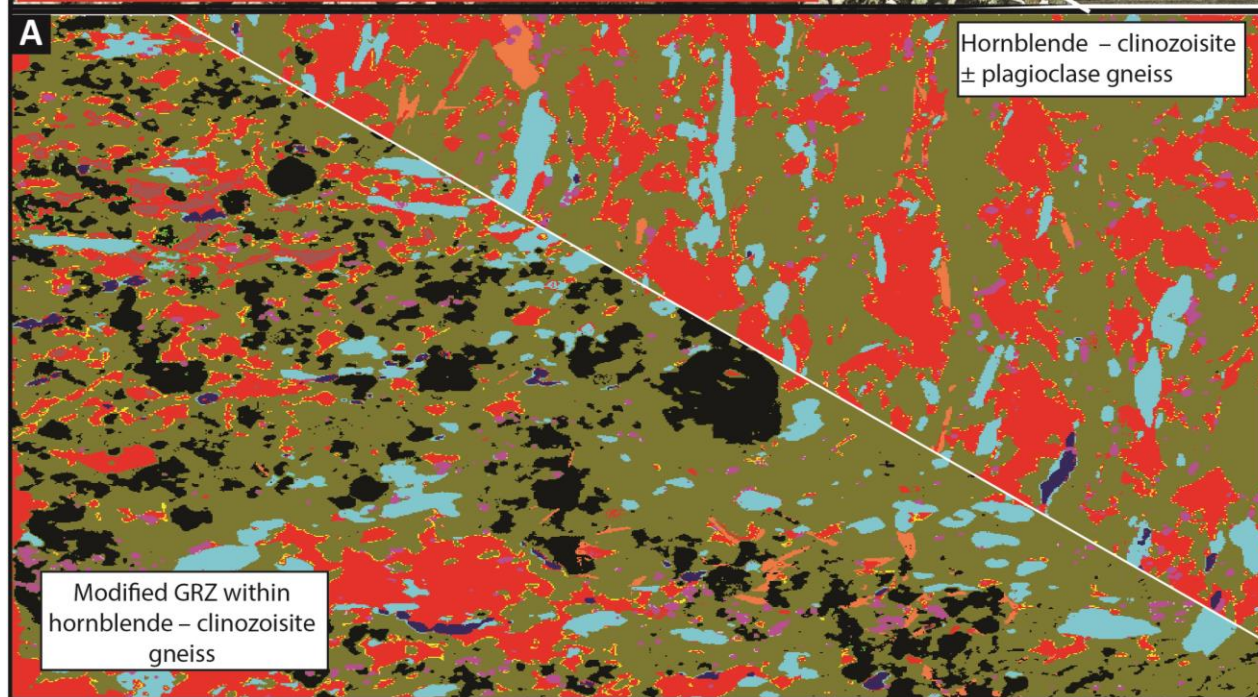
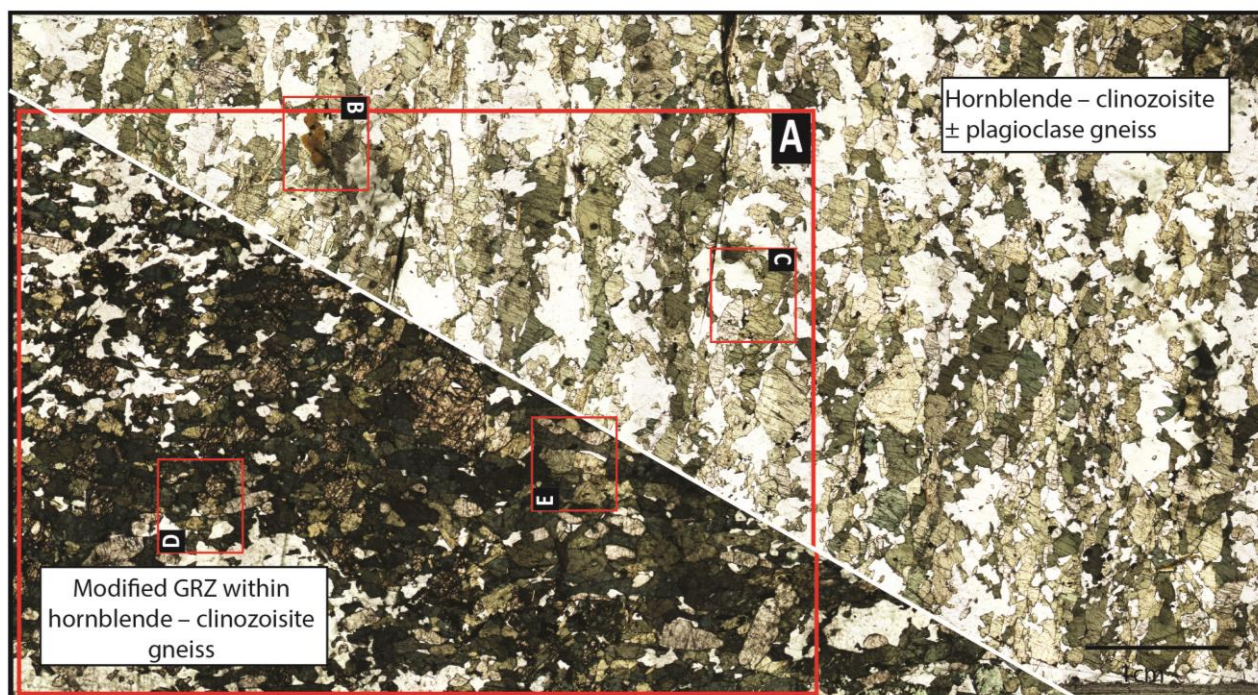
The remainder of the domain is made up of accessory rutile (0.98%), ilmenite (0.85%) titanite (2.56%), apatite (0.31%) and biotite (1.35%). Titanium-bearing minerals are found throughout the domain and are not attached to a single mineral. Apatite is also a minor component of this domain, scattered randomly throughout with a variable grain size. Biotite usually demonstrates a euhedral crystal structure and ranges from 1–3 mm in size and is usually bordering plagioclase.

**Figure 9 – Hornblende – clinozoisite gneiss + plagioclase - PV1703B and associated Modified GRZ – PV1704**

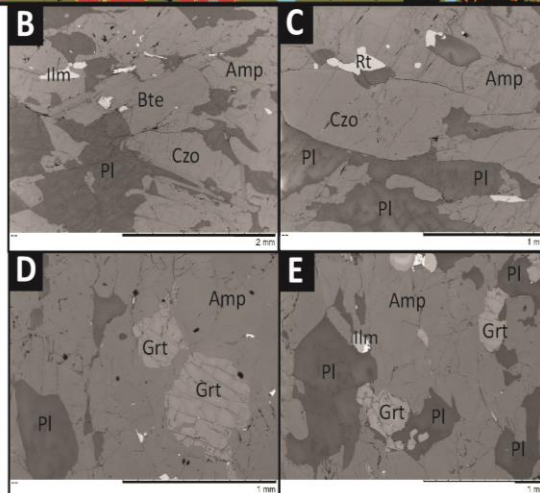
Modal percentages have been normalised to 100% for each domain to allow for direct comparison between samples

- A. u-XRF Mineral Map - the lower half of the sample is weakly modified GRZ domain while the upper half is weakly modified host domain
- B. BSE image showing textural relationships between Pl, Bt, Czo, Amp and Ilm within garnet poor region
- C. BSE image showing textural relationships between Pl, Bt, Czo, Amp and Rt within garnet poor region
- D. BSE image showing textural relationships between Pl, Grt and Amp within GRZ
- E. BSE image showing textural relationships between Pl, Grt and Amp within GRZ





Mineral	Area	
	Host	GRZ
Amphibole	54.75	52.42
Plagioclase	31.24	15.06
Clinozoisite	7.70	7.67
Garnet	0.00	15.69
Apatite	0.31	0.86
Biotite	1.35	1.04
Rutile	0.98	1.00
Ilmenite	0.85	0.93
Titanite	2.56	4.31
Quartz	0.25	1.05
Clinopyroxene	0.00	0.00
Other	0.00	0.00
Total	100.00	100.00





### Hornblende – clinozoisite ± plagioclase gneiss – PV1705B1

PV1705B1 is also part of the intermediate strain zone containing two domains (Figure 6D). Figure 10 demonstrates this split between the two domains; the lower GRZ and upper garnet-poor domain of this sample.

The GRZ domain of this sample is comprised of: amphibole (49.10%) which is distributed evenly throughout the domain; it appears to be randomly orientated with a grain size ranging from 2–4 mm. Plagioclase (12.74%) found in this GRZ domain has <1.5mm grain size. Clinozoisite (8.90%) is optically zoned with a distinct core and rim; grains range in size from 2–4 mm and are randomly orientated. As mentioned, garnet (26.34%) is found in the GRZ domain of this sample and are 1–4 mm in size (Figure 10C). Most of the garnets are fractured; these cracks contain amphibole and plagioclase (Figure 10B). The remainder of this domain is made up of rutile (0.56%), ilmenite (1.60%), titanite (0.03%), apatite (0.69%), quartz (0.02%) and others not able to be identified (0.01%). The titanium-bearing minerals are associated with the garnet (Figure 10B,C).

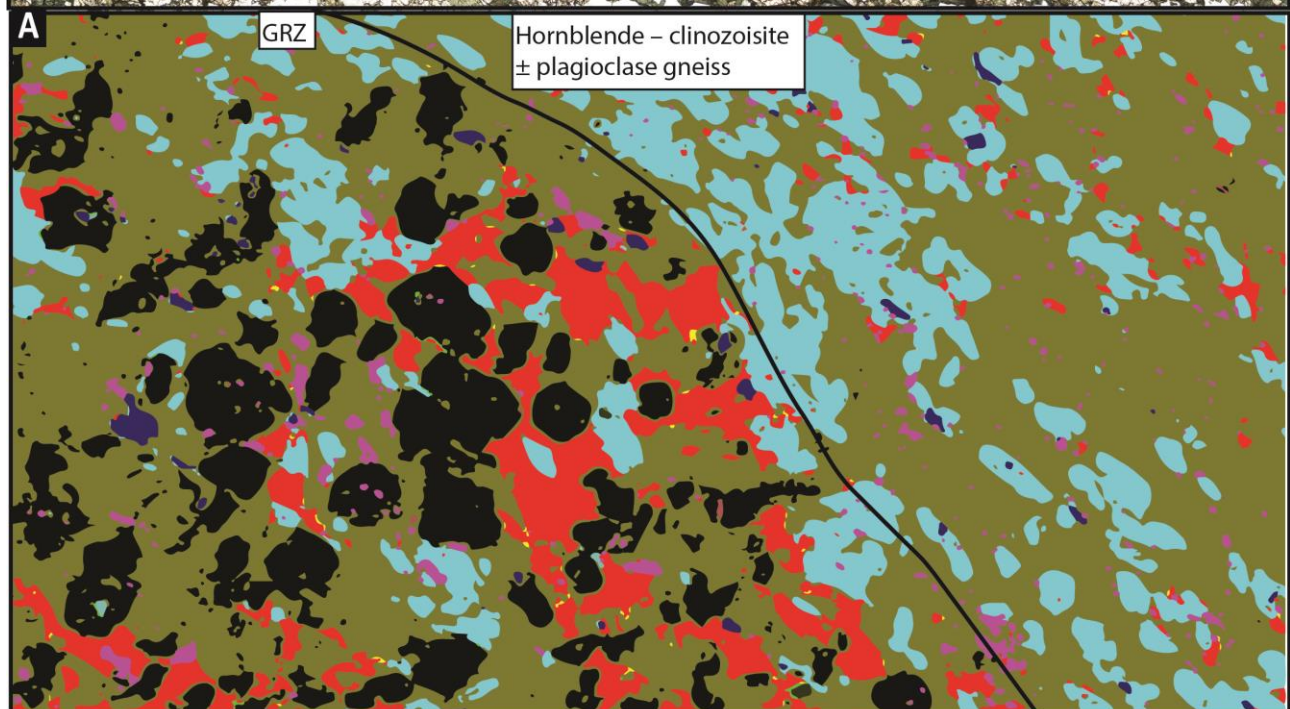
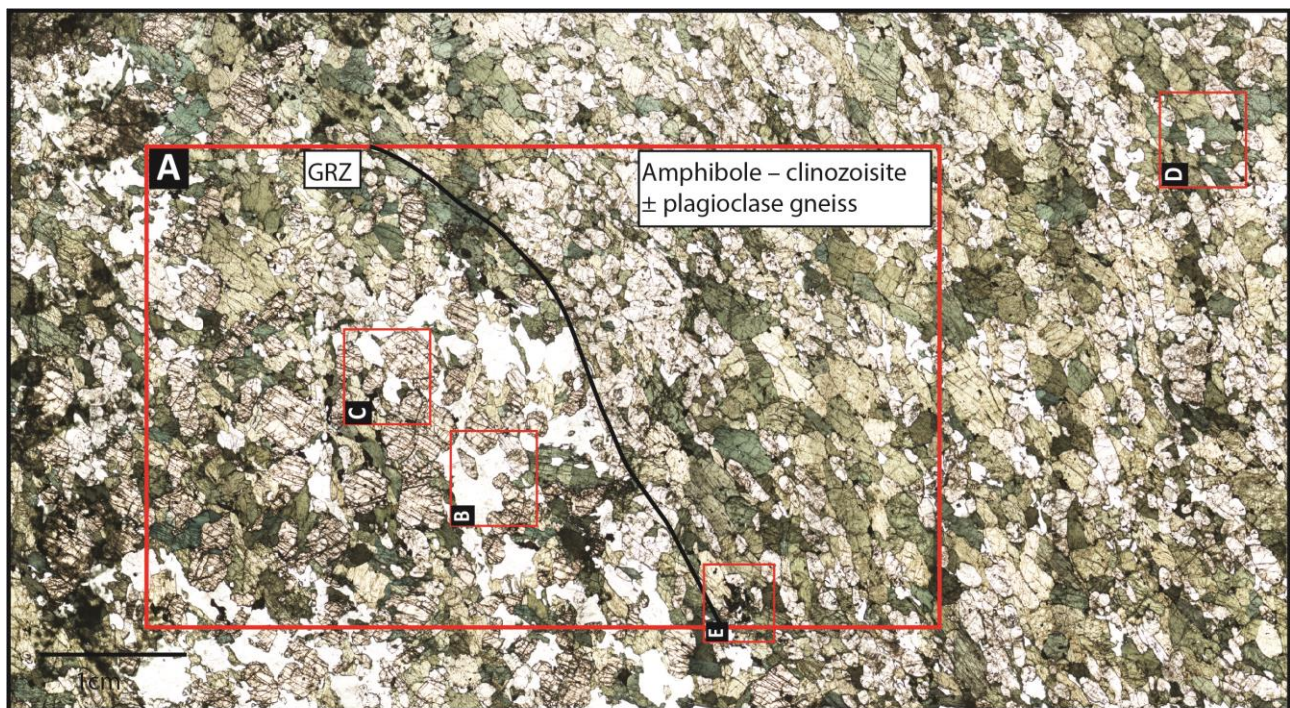
The garnet poor domain of this sample is comprised of amphibole (64.67%) and clinozoisite (27.47%). Both of which appear to have a slight alignment to them, and a similarly coarse grain size of 2–5mm. Plagioclase (4.39%) is randomly distributed through this section of the sample with a small grain size (Figure 10D). The remainder of this region is made up of rutile (0.51%), ilmenite (1.45%), titanite (0.03%), apatite (0.58%) and others not able to be identified (0.02%) (Figure 10E). Apatite is scattered randomly throughout the sample with a variable grain size.

#### **Figure 10** – Hornblende – clinozoisite ± plagioclase gneiss – PV1705B1

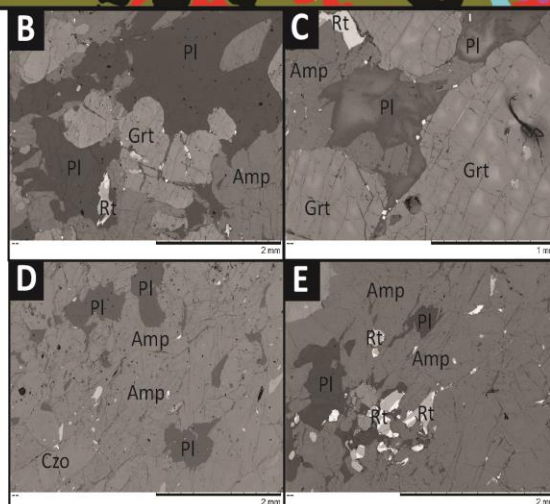
Modal percentages have been normalised to 100% for each domain to allow for direct comparison between samples

- A. u-XRF Mineral Map - the lower half of the sample is weakly modified GRZ domain while the upper half is weakly modified host domain
- B. BSE image showing textural relationships between Pl, Amp, Rt and Grt within the GRZ
- C. BSE image showing textural relationships between Pl, Amp, Rt and Grt within the GRZ
- D. BSE image showing textural relationships between Pl, Amp and Czo within garnet poor region
- E. BSE image showing textural relationships between Pl, Amp and Rt within garnet poor region





PV1705B1	Area %	
Mineral	Host	GRZ
Amphibole	64.67	49.10
Plagioclase	4.39	12.74
Clinozoisite	27.47	8.90
Garnet	0.86	26.34
Apatite	0.58	0.69
Biotite	0.00	0.00
Rutile	0.51	0.56
Ilmenite	1.45	1.60
Titanite	0.03	0.03
Quartz	0.01	0.02
Clinopyroxene	0.00	0.00
Other	0.02	0.02
Total	100.00	100.00



### Hornblende-clinozoisite gneiss – PV1708

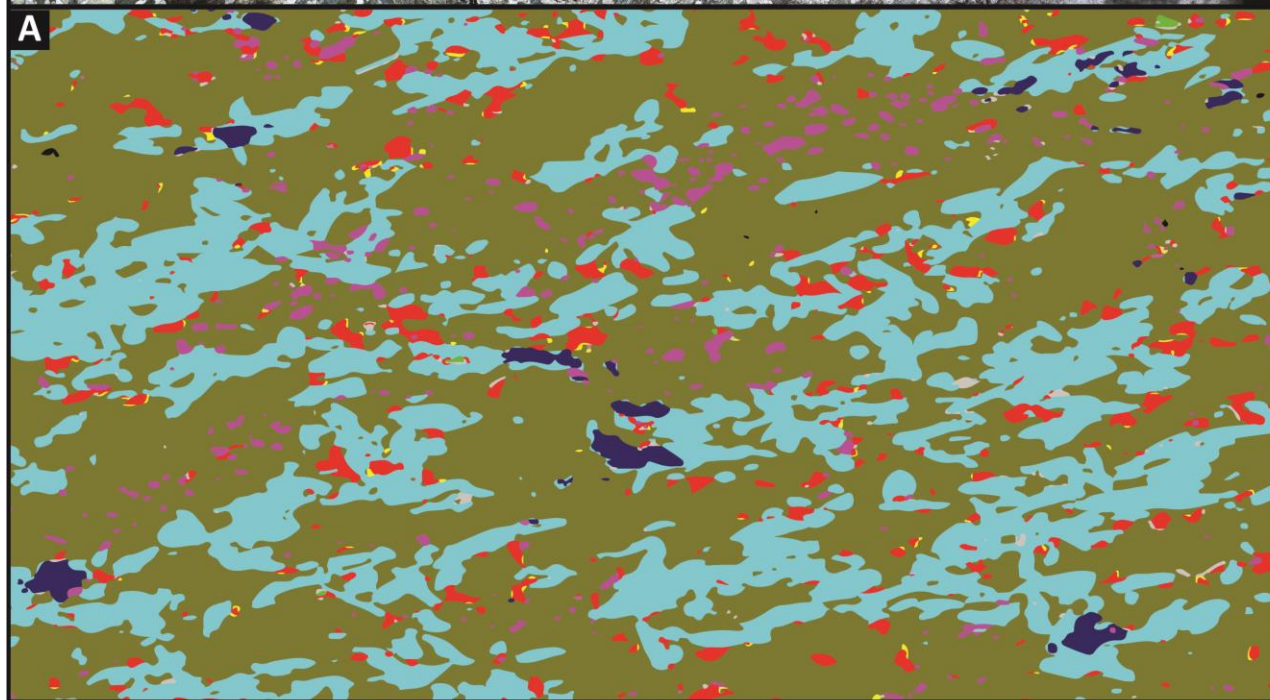
This sample is located in an area of the field site that is very garnet poor with no GRZ within 2–3 m of it and is a heavily modified version of the two-pyroxene-pargasite gneiss. PV1708 is a region of the Pembroke Valley that is comprised of two main minerals and 4 minor minerals; the major components are amphibole (62.49%) and clinozoisite (28.79%), with minor minerals being plagioclase (6.90%), rutile (0.78%), ilmenite (1.16%), titanite (0.03%), apatite (1.14%) and garnet (0.04%) (Figure 11).

Amphibole is distributed evenly throughout the sample; it is randomly orientated, anhedral, with a grain size ranging from 2–3 mm. Clinozoisite is optically zoned. Grains range in size from 1–2 mm and have a slight alignment to them. Plagioclase does not show any complex zonation textures, with a grain size that is <1.5 mm (Figure 11B). The remainder of the sample is made up of accessory rutile, ilmenite, titanite, apatite and garnet. The titanium bearing minerals are found throughout the sample and appear to be in slight alignment (Figure 11B, C, D & E). Apatite is scattered randomly throughout the sample with a variable grain size. Garnet is a very small component of this sample and is very difficult to identify due to its small grain size.

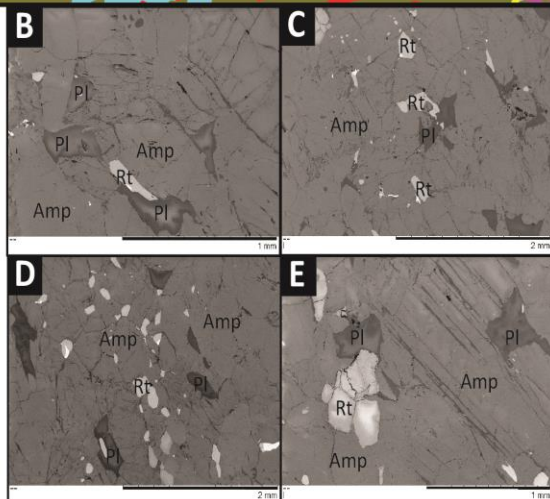
#### **Figure 11** – Hornblende – clinozoisite gneiss – PV1708

- A. u-XRF Mineral Map of amphibole – clinozoisite gneiss– PV1708
- B. BSE image showing textural relationships between Pl, Amp and Rt within the amphibole – clinozoisite gneiss
- C. BSE image showing textural relationships between Pl, Amp and Rt within the amphibole – clinozoisite gneiss
- D. BSE image showing textural relationships between Pl, Amp and Rt within the amphibole – clinozoisite gneiss
- E. BSE image showing textural relationships between Pl, Amp and Rt within the amphibole – clinozoisite gneiss





PV1708	Area %
Mineral	Total
Amphibole	62.49
Plagioclase	6.90
Clinozoisite	28.79
Garnet	0.04
Apatite	1.14
Biotite	0.00
Rutile	0.78
Ilmenite	1.16
Titanite	0.03
Quartz	0.00
Clinopyroxene	0.00
Other	0.00
Total	101.32



### Steeply dipping high strain zone – PV1702C1

A steeply dipping D<sub>3</sub> high strain zone is exposed in a 2–4 m wide band running through the study area (Figure 7B). This unit is the highest strain rock and is most modified and as a result the modified GRZ are difficult to distinguish (Figure 12). The garnet-rich domains are very garnet poor when compared to other samples in the field site. However, when compared to the rest of this sample they are enriched in garnet.

Within the garnet-rich domains, amphibole (64.09%) is coarse grained ranging in size from 2–5 mm and is found across the region, there also appears to be an alignment with these areas, while some grains demonstrate crystal faces (Figure 12C). Plagioclase (16.99%) is also coarse grained, ranging in size from 1–3mm. Clinozoisite (12.57%) is scattered throughout these domains and ranges in size from fine (<1mm) to coarse grained (>7mm). It occurs within plagioclase and amphibole grains as well as along the boundaries of these two minerals. The coarser clinozoisite grains are elongate in the same orientation as the amphibole grains. Some of the clinozoisite grains are also optically zoned (Figure 12B). Garnet is a very minor mineral in these regions and accounts for 2.05% of the sample. The garnet is messy with large cracks and areas that have been infilled with an assortment of mineral phases (amphibole, plagioclase and rutile) (Figure 12D). Those garnets that are not messy demonstrate crystal faces. The remainder of this garnet rich area is comprised of rutile (0.68%), ilmenite (0.85%), titanite (0.2.14%) and apatite (0.64%).

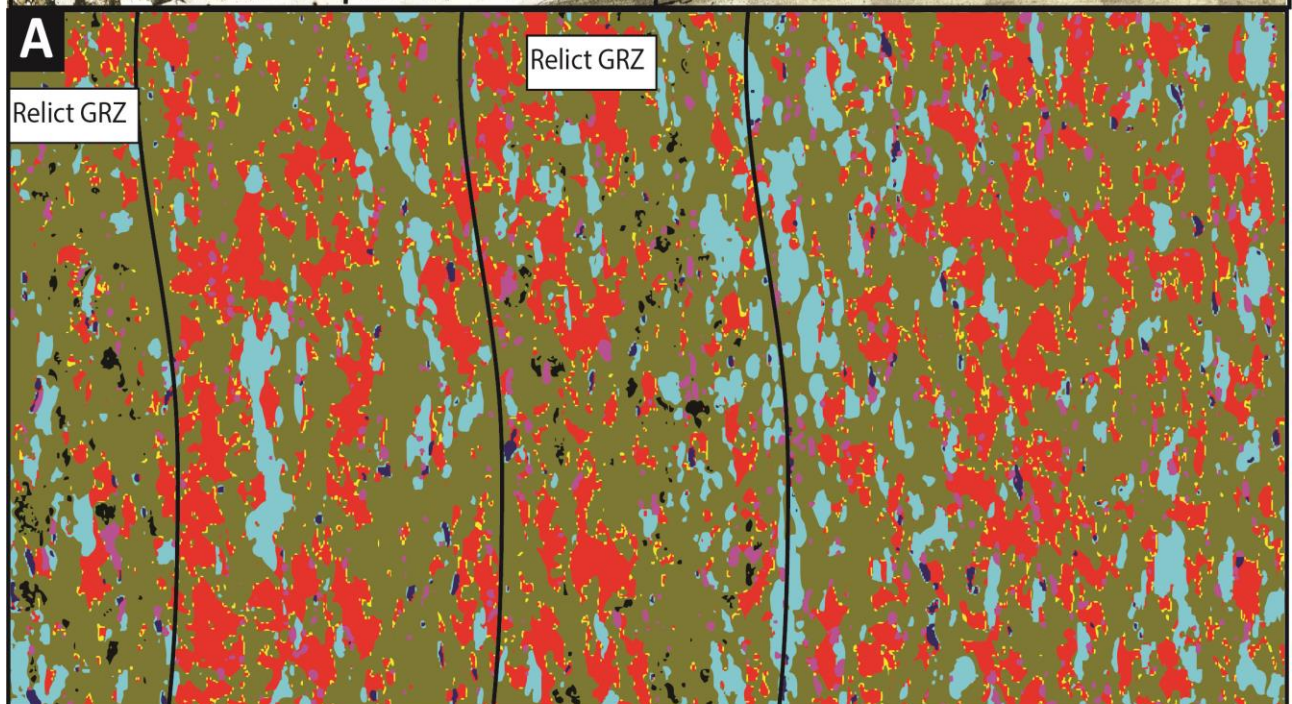
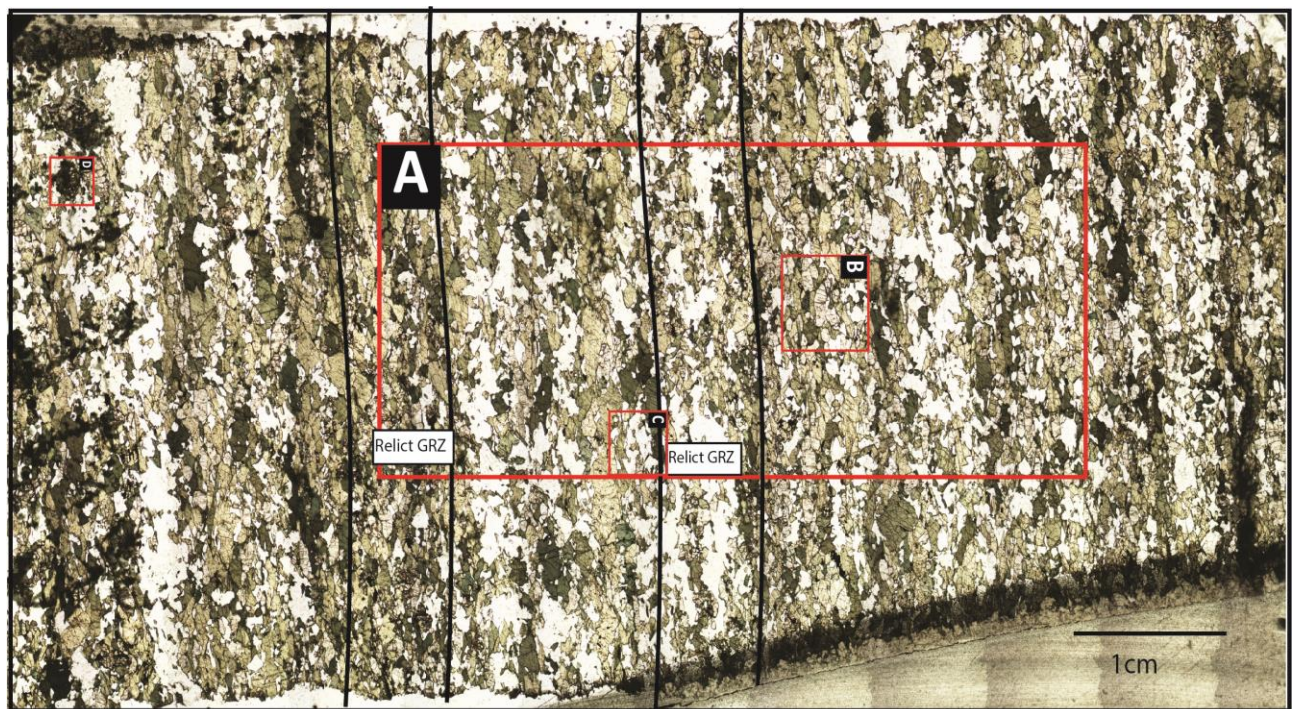
The remainder of the sample is the garnet-poor domain and is comprised of amphibole (58.18%) and similarly to the garnet rich domain there is an alignment to these grains, plagioclase (24.20%) and clinozoisite (11.62%). Rutile (0.96%), ilmenite (1.44%), titanite (2.88%) and apatite (0.72%) make up the remainder of this sample. The apatite is scattered randomly throughout the sample with a variable grain size.

#### **Figure 12** – Steeply dipping high strain zone – PV1702C1

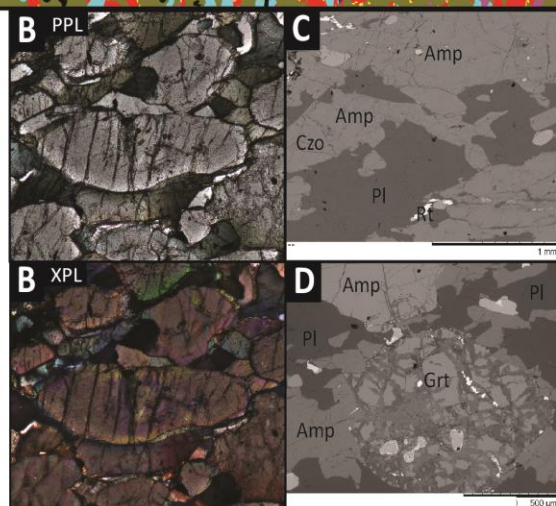
Modal percentages have been normalised to 100% for each domain to allow for direct comparison between samples

- A. u-XRF Mineral Map – Steeply dipping high strain zone – PV1702C1 – showing relict GRZ and modified host rock
- B. Photomicrograph of optically zoned clinozoisite grain under PPL and XPL
- C. BSE image showing textural relationships between Pl, Amp and Czo within the modified host rock
- D. BSE image showing textural relationships between Pl, Amp and Grt within the modified host rock





PV1702C1		
	Area %	
Mineral	Host	GRZ
Amphibole	58.18	64.09
Plagioclase	24.20	16.99
Clinozoisite	11.62	12.57
Garnet	0.00	2.05
Apatite	0.72	0.64
Biotite	0.00	0.00
Rutile	0.96	0.68
Ilmenite	1.44	0.85
Titanite	2.88	2.14
Quartz	0.00	0.00
Clinopyroxene	0.00	0.00
Other	0.00	0.00
Total	100.00	100.00





## Modification due to strain

As strain increases, a pattern relating to the modes of the four major minerals (amphibole, plagioclase, clinozoisite and garnet) is evident. As can be seen in Figure 13, with increasing strain there is also an increase in amphibole modal percentage across both the GRZ and host domains, from 30–40% in the modified precursor rock to >55% in the highest strained and modified samples. Plagioclase decreases its abundance from low strain (45–50%) to moderate strain samples (30–<10%). However, the sample from the steeply dipping high strain zone demonstrates an increase in the plagioclase abundance (15–25%) compared with the intermediate strain rocks. Clinozoisite also increases in abundance from the weakly modified two-pyroxene-plagioclase gneiss (1%) to the moderately strained hornblende-clinozoisite gneiss (30% in the host domain, and  $\approx$  10% in the GRZ domains). In the host domains of the high strained rock, this decreases to about 10%, although in the GRZ domain it increases to >10%. Garnet does not show much correlation between the host domains of the modified rocks. In the GRZ domains, garnet doesn't really increase in abundance across the low to moderate strain samples. However, there is a significant decrease in garnet abundance in the high strain sample.

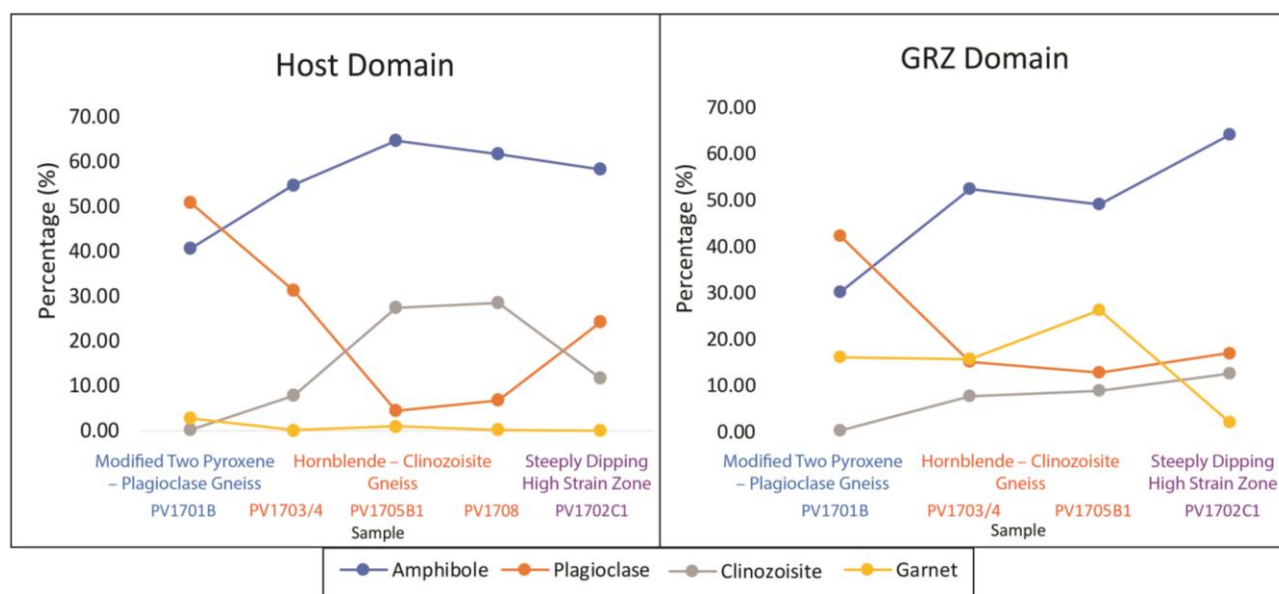


**Figure 13** – Graph illustrating the changes in mineral abundances as strain rates increase

Sample PV1708 does not have a GRZ domain so has been omitted of the GRZ graph

Modal percentages have been normalised to 100% for each domain to allow for direct comparison

## Microstructures

Five distinct microstructures are identified and are distributed across all representative samples.

### Small ( $\leq 60^\circ$ ) dihedral angles of interstitial grains (plagioclase, ilmenite, rutile & clinozoisite)

The most common key microstructure found in the field site is low ( $\leq 60^\circ$ ) apparent dihedral angles. This microstructure is found at the junction of three distinct mineral grains of varying combinations. Mineral combinations found within this field site are amphibole-ilmenite-amphibole (Figure 14.1, 16.6), amphibole-plagioclase-amphibole (Figure 14.2, 15.3, 16.2, 17.3 & 19.2), amphibole-plagioclase-apatite (Figure 14.3), amphibole-rutile-amphibole (Figure 15.5), amphibole-clinozoisite-amphibole (Figure 15.1 & 16.1), rutile-plagioclase-amphibole (Figure 16.1 & 19.4), clinozoisite-plagioclase-clinozoisite (Figure 16.4 & 18.1), plagioclase-rutile-plagioclase (Figure 17.1), rutile-plagioclase-garnet (Figure 17.1), garnet-plagioclase-garnet (Figure 17.5), amphibole-plagioclase-clinozoisite (Figure 18.5 & 19.5), and rutile-plagioclase-apatite (Figure 19.1). The small dihedral angle may occur as terminations of elongate grains or as cusped boundaries of grains at triple point junctions. In some circumstances the small dihedral angles may continue into veinlets along grain boundaries.

### Veinlets and elongate interstitial grains (plagioclase, rutile, clinozoisite)

Veinlets and elongate interstitial grains of mainly plagioclase and less commonly clinozoisite and rutile are found between grains of contrasting minerals. Films of plagioclase are associated with grain boundaries involving the following minerals: amphibole (Figure 15.4, 16.5, 17.2, 18.6, 19.3 & 19.8), garnet (Figure 15.2), biotite (Figure 16.6), apatite and clinozoisite (Figure 18.3 & 19.7), clinozoisite and amphibole (18.4) and clinozoisite (Figure 18.7). Elongate plagioclase on amphibole grain boundaries terminate with finely tapered ends with consistently small apparent dihedral angles. Veinlets of clinozoisite can also be found in the samples, although is a lot scarcer than its plagioclase counterpart. It is associated with garnet in Figure 15.1.

### Melt pseudomorphs

Single-mineral feldspar pseudomorphs of biotite are found throughout several of the samples (Figure 15.7, 16.6). These grains tend to be coarse grained at 1–2 mm in size. In other samples, plagioclase is replacing amphibole and clinozoisite (Figure 18.8).

### Cusped grains

Cusped areas (concave outward) of plagioclase can be found throughout the samples and involves plagioclase and amphibole (Figure 14.4, 15.6, 17.4, 18.2 & 19.6). This microstructure tends to be very subtle and ranges in size from <0.5mm to 1 mm.

## Symplectites

Symplectic replacement aggregates and coronas are found in one sample (weakly modified two-pyroxene-pargasite gneiss. Here, the symplectites are comprised of amphibole, clinozoisite and plagioclase, and surround an inner clinopyroxene grain (Figure 14.5). Symplectite textures are very rare in all intermediate and high strain samples.

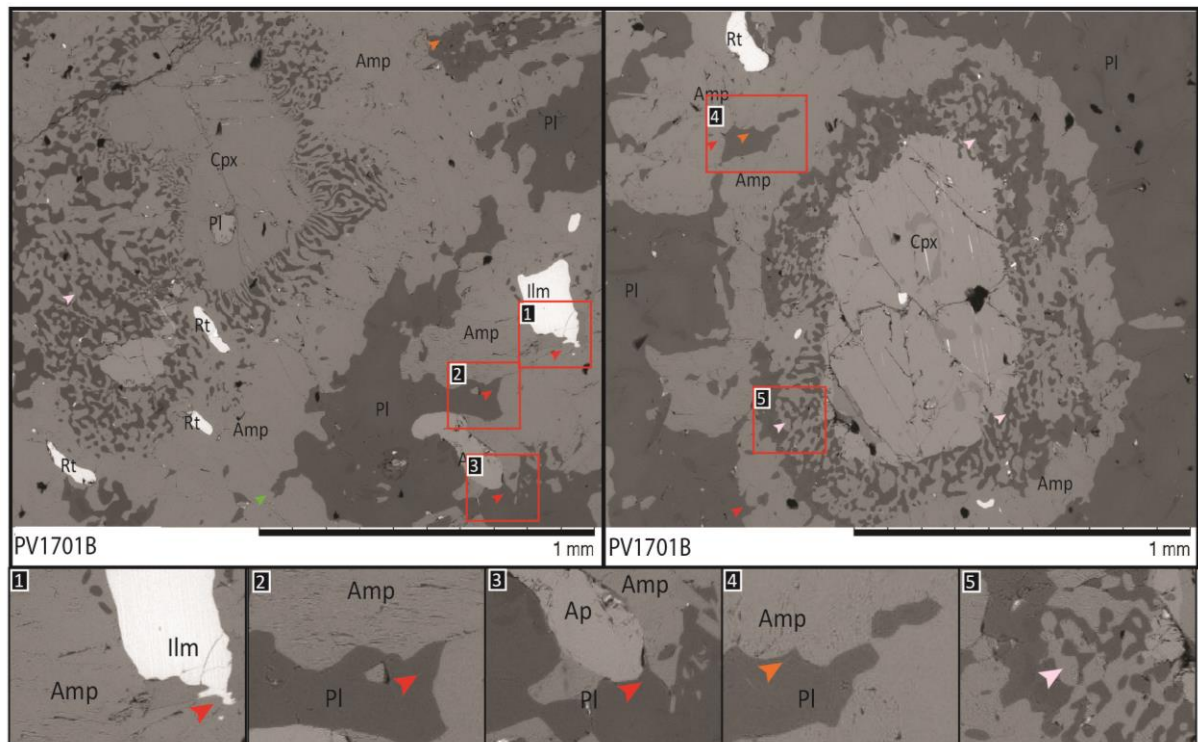


**Figure 14** – BSE images of weakly modified two pyroxene – plagioclase gneiss – PV1701B

1- Low dihedral angle at Amp, Ilm, Amp junction (red), 2- Low dihedral angle at Amp, Pl, Amp junction (red), 3- Low dihedral angle at Amp, Pl, Ap junction (red), 4- Cuspate outwards grain boundary involving Amp and Pl (orange), 5- Symplectic replacement aggregates involving Amp and Pl (white)

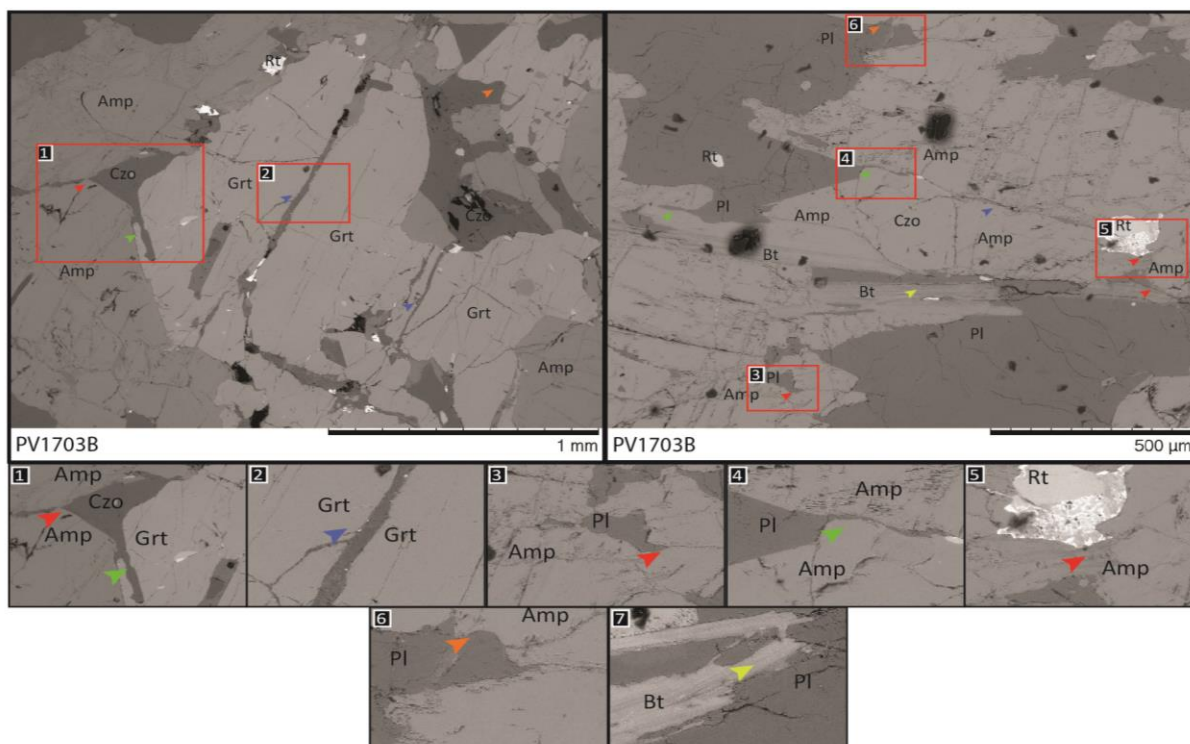


**Figure 15** – BSE images of hornblende – clinozoisite gneiss + plagioclase - PV1703B

1 - Low dihedral angle at Amp, Czo, Amp boundary (red) and a veinlet of Czo infiltrating along a crack in Grt (green), 2- Melt film of Pl along a crack in Grt (blue), 3- Low dihedral angle at Amp, Pl, Amp (red), 4 – Veinlet of Pl infiltrating along Amp grain boundary (green), 5 - Low dihedral angle at Amp, Rt, Amp boundary (red), 6 - Cusped outwards grain boundary, involving Pl and Amp (orange), 7- Melting of Bt by melt which is being pseudomorphed by Pl (yellow)

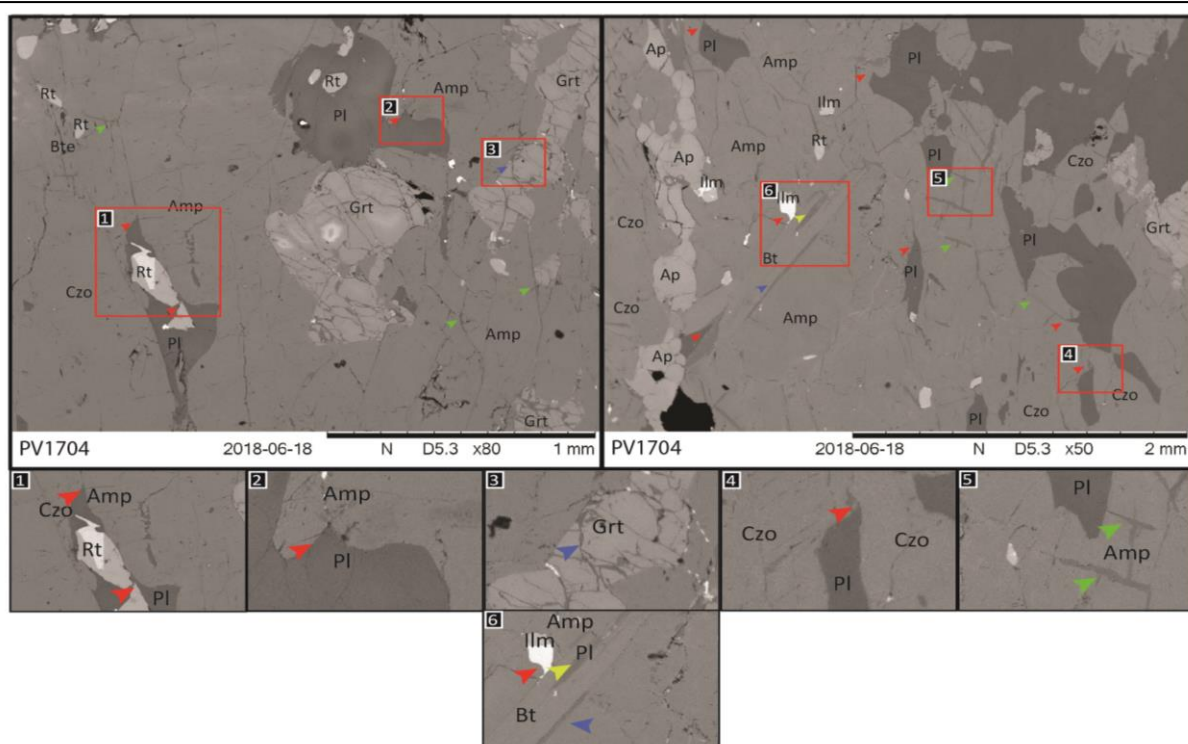


**Figure 16** – BSE images of modified GRZ within hornblende – clinozoisite gneiss – PV1704

1 - Low dihedral angle at Amp, Czo, Amp boundary and at Rt, Pl, Amp boundary (red), 2- Low dihedral angle at Amp, Pl, Amp boundary (red), 3- Melt film of Pl along cracks in Grt (blue), 4 – Low dihedral angle at Czo, Pl, Czo boundary (red), 5 – Veinlets of Pl infiltrating along Amp grain boundaries (green), 6 – Low dihedral angle at Amp, Ilm, Amp boundary (red), Melting of Bt by melt which is being pseudomorphed by Pl (yellow), melt film of Pl along Bt grain boundary (blue).



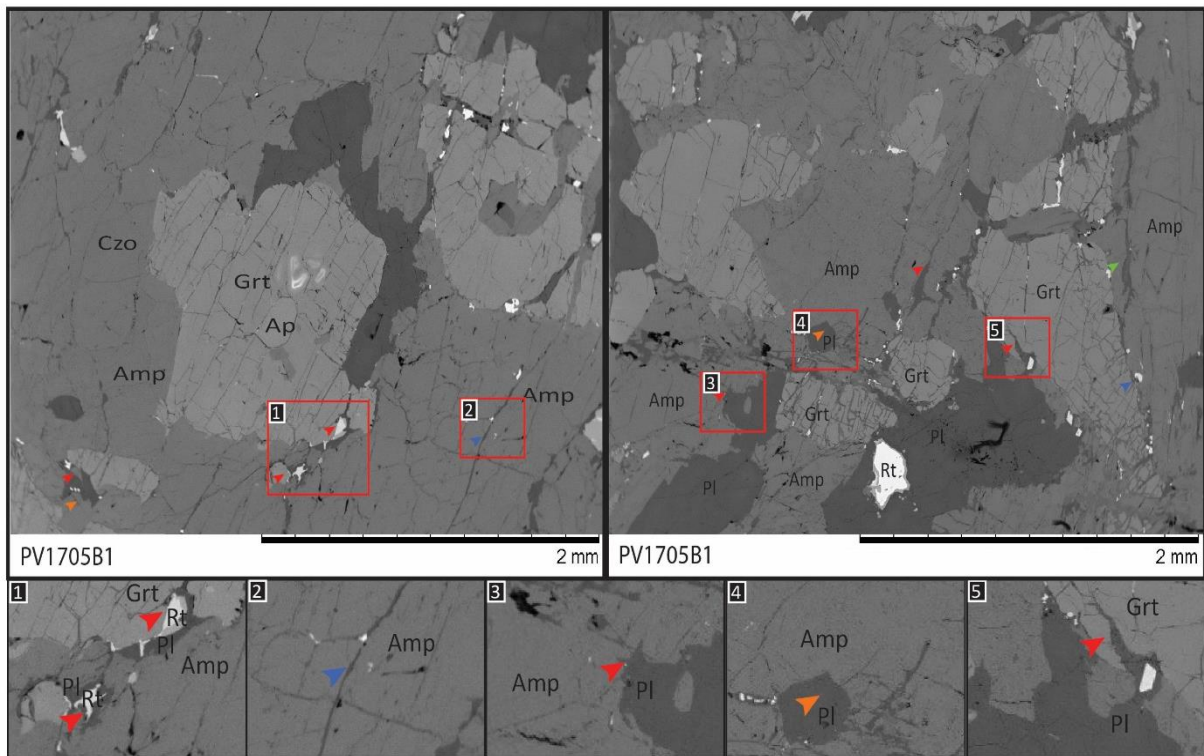


**Figure 17** – BSE images of hornblende – clinozoisite ± plagioclase gneiss – PV1705B1

1 - Low dihedral angle at Pl, Rt, Pl boundary and at Rt, Pl, Grt boundary (red), 2- Melt film of Pl along Amp grain boundary (blue), 3 - Low dihedral angle at Amp, Pl, Amp (red), 4 – Cuspate outwards grain boundary involving Pl and Amp (orange), 5 – Low dihedral angle at Grt, Pl, Grt boundary

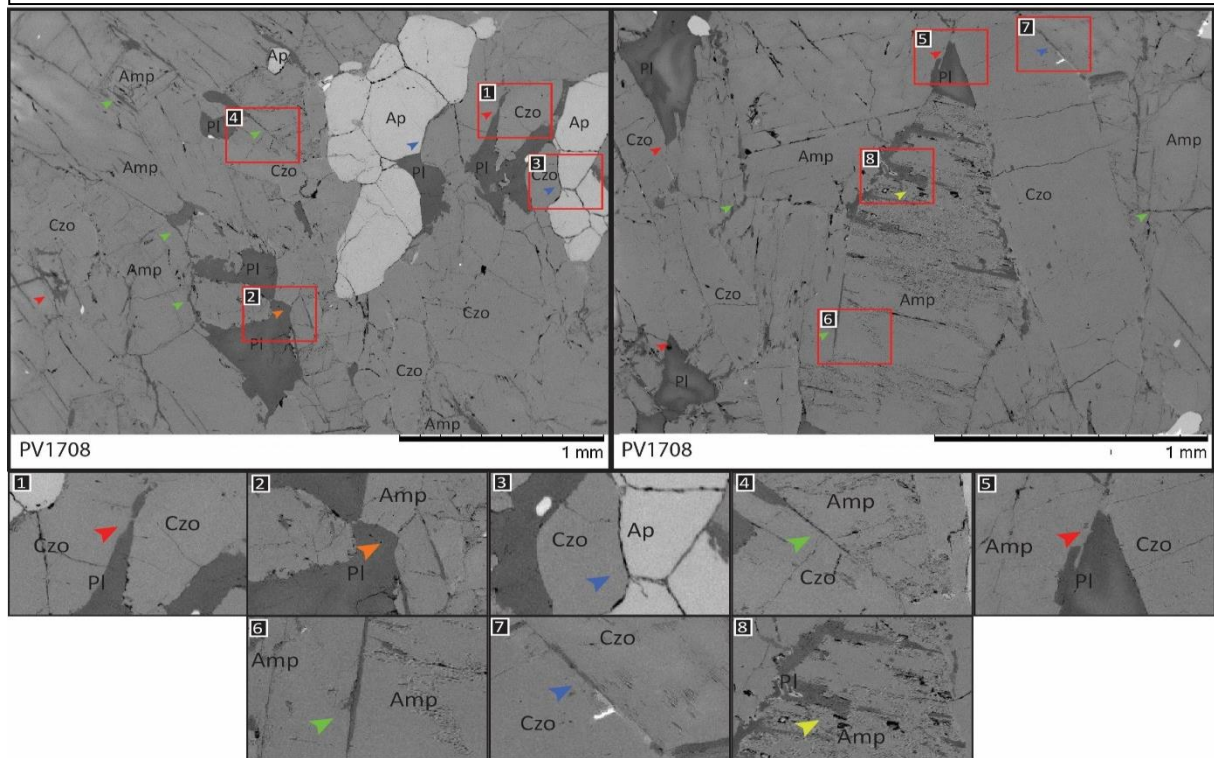


**Figure 18** – BSE images of hornblende – clinozoisite gneiss - PV1708

1 - Low dihedral angle at Czo, Pl, Czo boundary (red), 2 - Cuspate outwards grain boundary involving Pl and Amp (orange), 3 – Melt film of Pl along Czo and Ap grain boundary (blue), 4 – Veinlet of Pl infiltrating along Amp and Czo grain boundary (green), 5 - Low dihedral angle at Amp, Pl, Czo boundary (red), 6 – Veinlet of Pl infiltrating along Amp grain boundary (green), 7 - Melt film of Pl along Czo grain boundary (blue), 8 - Melting of Amp by melt which is being pseudomorphed by Pl (yellow)

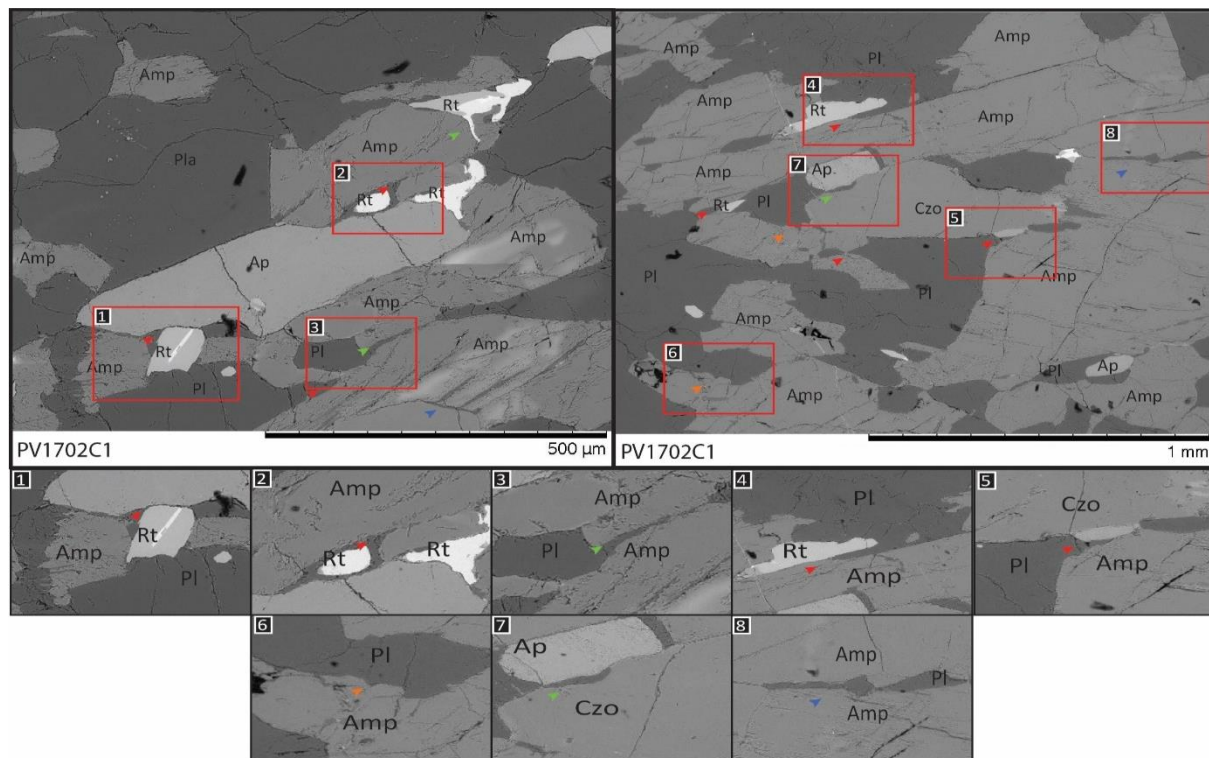


**Figure 19** – BSE images of steeply dipping high strain zone – PV1702C1

1 - Low dihedral angle at Rt, Pl, Ap boundary (red), 2- Low dihedral angle at Amp, Pl, Amp boundary (red), 3- Veinlet of Pl infiltrating along Amp grain boundary (green), 4 - Low dihedral angle at Rt, Pl, Amp boundary (red), 5 - Low dihedral angle at Amp, Pl, Czo boundary (red), 6 - Cusped outwards grain boundary, involving Pl and Amp (orange), 7- Veinlet of Pl infiltrating along Ap, Czo grain boundary (green), 8 - Melt film of Pl, along Amp grain boundary (blue)

## Zircon Analysis

### U-Pb geochronology

#### Weakly modified two-pyroxene – plagioclase gneiss – PV1232 (Elliot, 2016)

Zircons from the weakly modified two-pyroxene-plagioclase gneiss lack well-formed crystal faces and have varied morphologies ranging from rounded to irregular (Figure 20A). Internal structures range from sector, oscillatory, planar to homogenous zoning in CL. U-Pb analyses made on 19 grains from the host two-pyroxene-plagioclase gneiss give  $^{206}\text{Pb}/^{238}\text{U}$  ages ranging from c. 127.5 Ma to 136.8 Ma, this spread of concordant age data used a large proportion of the two minute LA-ICP-MS analysis signal. The weighted mean for all 19 grains is  $130.93 \pm 0.36$  Ma ( $2\sigma$ ) with a high MSWD of 1.70, suggesting this is not a single population (Figure 21). The same 19 grains also give a concordia age of  $130.97 \pm 0.35$  Ma but with a low MSWD of 0.16 ( $2\sigma$ ) (Figure 22A). This indicates the  $130.97 \pm 0.35$  age is likely an under estimation and can be regarded as a minimum age of crystallisation. The smear of ages lacking a flat region on the weighted mean plot suggests Pb-loss or partial recrystallization to varying degrees in all grains. CL images show no consistent correlation in internal structures to  $^{206}\text{Pb}/^{238}\text{U}$  ages. Chi-square value of 0.028 which is <95% confidence suggests that the ages given by these samples is geologically questionable.



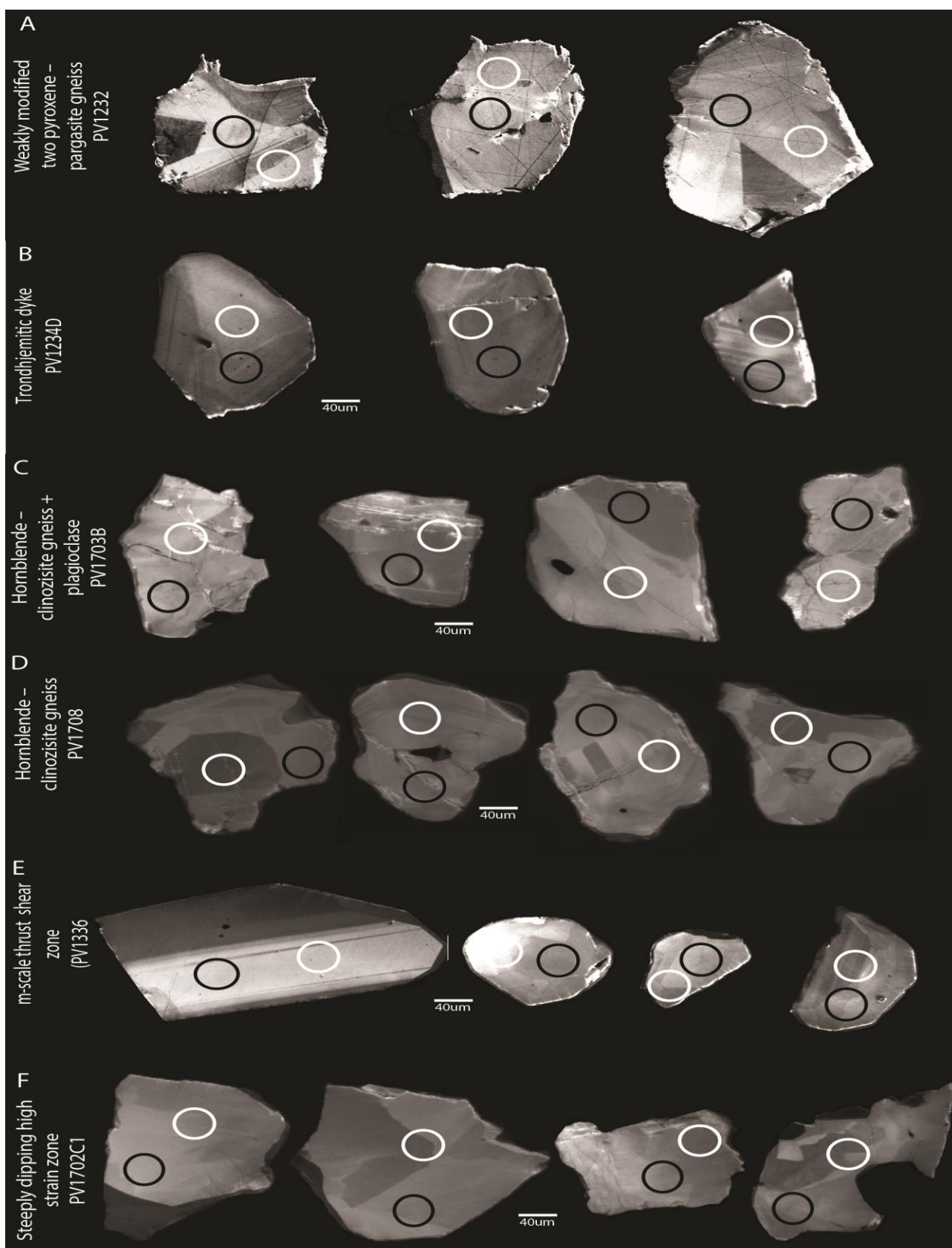
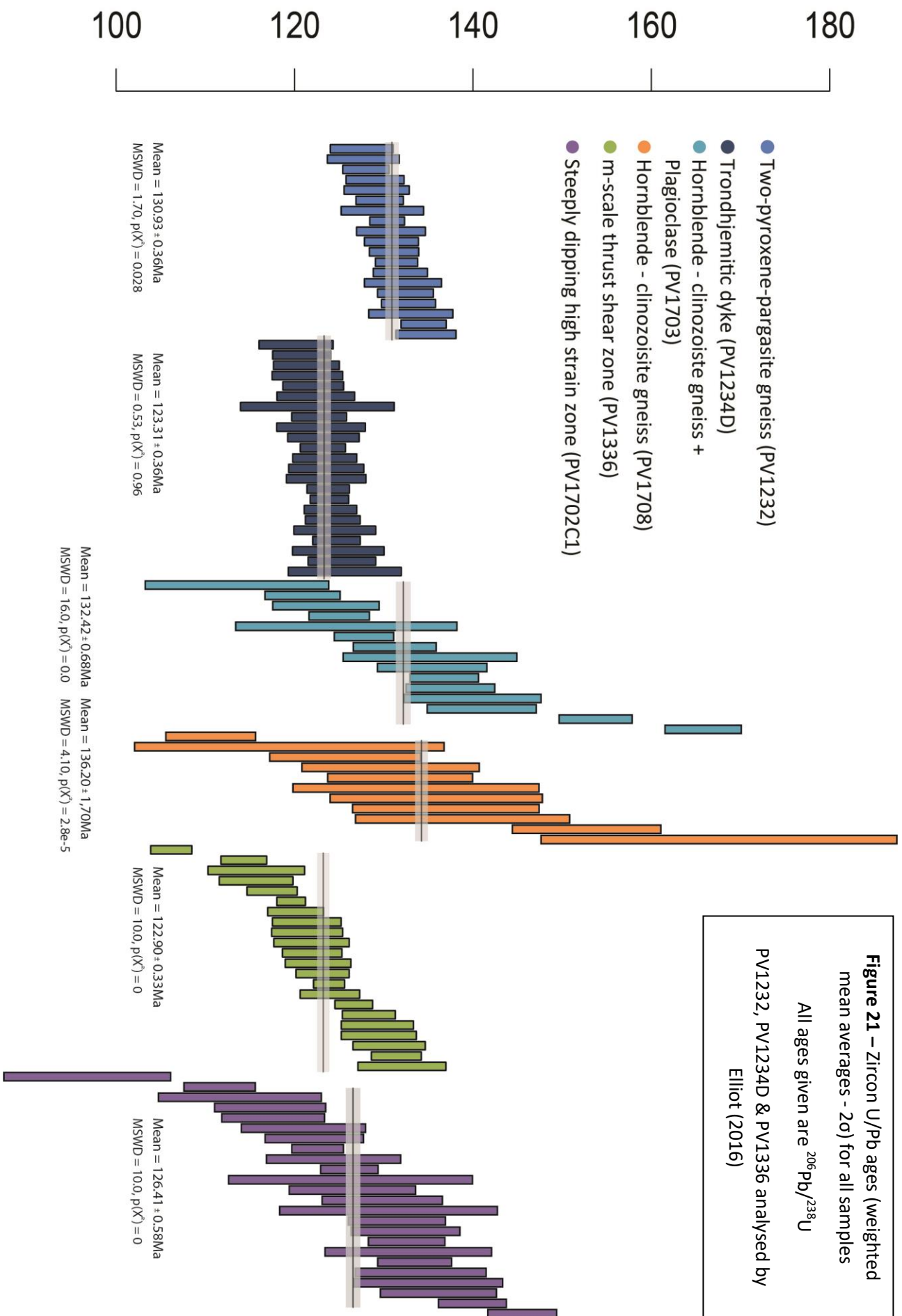


**Figure 20** - Cathodoluminescence images of representative zircons from all samples

Black circles represent areas from where trace element data was obtained from

While white circles represent where U/Pb data was obtained from (PV1232, PV1234D & PV1336 analysed by Elliot (2016))





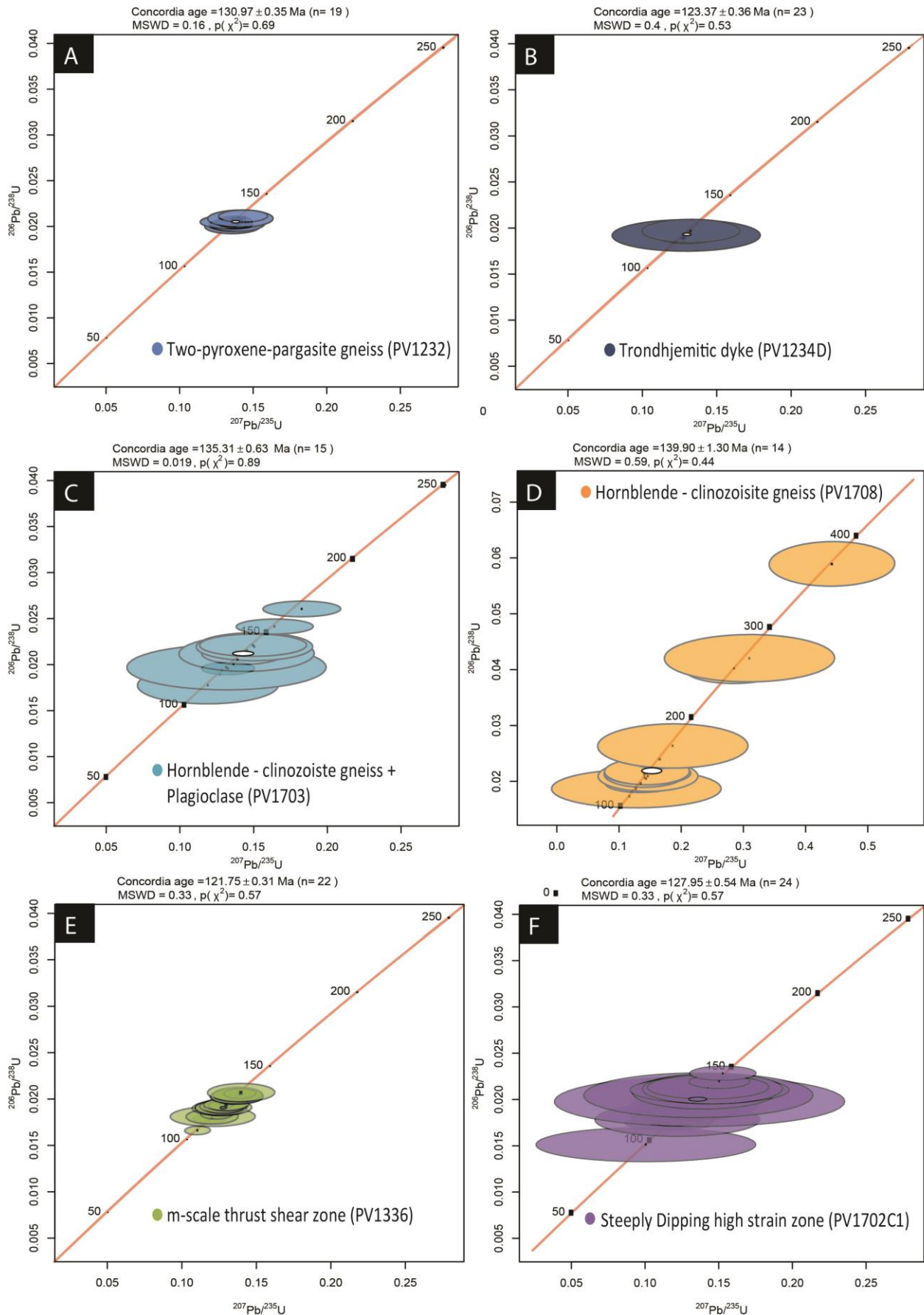


**Figure 22 – Zircon U/Pb ages (Concordia plots) for all samples**

All ages given are  $^{206}\text{Pb}/^{238}\text{U}$

PV1232, PV1234D & PV1336 analysed by Elliot (2016)

#### Trondhjemitic dyke – PV1234D

Zircons from the trondhjemitic dyke lack well-formed crystal faces and have varied morphologies ranging from rounded to irregular (Figure 20B). They have internal structures ranging from sector, oscillatory, planar to homogenous in CL images. U-Pb analyses made on 23 grains from the trondhjemitic dyke give  $^{206}\text{Pb}/^{238}\text{U}$  ages ranging from c. 115.9 Ma to 129.1 Ma, this spread of concordant age data used a large proportion of the two minute LA-ICP-MS analysis signal. The weighted mean for all 23 grains is  $123.31 \pm 0.37$  Ma ( $2\sigma$ ) with a low MSWD of 0.53 suggests the observed scatter of ages is less than that predicted (Figure 21). The same 23 grains also give a concordia age of  $123.37 \pm 0.36$  Ma but with a low MSWD of 0.4 ( $2\sigma$ ) (Figure 22B). This indicates the  $123.37 \pm 0.36$  age is likely an under estimation and can be regarded as a minimum age of crystallisation. The constant smear of ages lacking a flat region on the weighted mean plot suggests Pb-loss or partial recrystallization to varying degrees in all grains. CL images show no consistent correlation in internal structures to  $^{206}\text{Pb}/^{238}\text{U}$  ages. A Chi-square value of 0.96 which is better than 95% confidence suggests that the age given by this sample is geologically meaningful and will be considered a reliable age determination representing the age of the dyking and GRZ-forming event.

#### Hornblende-clinzoisite-plagioclase gneiss – PV1703B

Zircons from the hornblende-clinzoisite-plagioclase gneiss lack well-formed crystal faces and have varied morphologies ranging from rounded to irregular (Figure 20C). Internal structures range from sector, oscillatory, planar to homogenous in CL images. 15 U-Pb analyses made on 18 grains from the hornblende-clinzoisite-plagioclase gneiss give  $^{206}\text{Pb}/^{238}\text{U}$  ages ranging from c. 113.5 Ma to 165.8 Ma, this spread of age data used very small proportion of the two minute LA-ICP-MS analysis signal to make it concordant. The weighted mean for 15 grains is  $132.42 \pm 0.36$  Ma ( $2\sigma$ ) with a low MSWD of 0.53 that suggests the observed scatter of ages is less than that predicted (Figure 21). The same 15 grains also give a concordia age of  $135.31 \pm 0.63$  Ma but with a low MSWD of 0.019 ( $2\sigma$ ) (Figure 22C). This indicates the  $135.31 \pm 0.63$  Ma age is likely an under estimation and can be regarded as a minimum age of crystallisation. The smear of ages lacking a flat region on the weighted mean plot suggest Pb-loss or partial recrystallization to varying degrees in all grains. CL images show no consistent correlation in internal structures to  $^{206}\text{Pb}/^{238}\text{U}$  ages. The Chi-square value of 0.89 which is  $> 95\%$  confidence suggests that the age given by this sample is geologically meaningful and will be considered a reliable age prediction (Figure 21).

### Hornblende-clinozoisite gneiss – PV1708

Zircons from the hornblende-clinozoisite gneiss lack well-formed crystal faces and show varied morphologies ranging from rounded to irregular (Figure 20d). Internal structures range from sector, oscillatory, planar to homogenous in CL images. 14 U-Pb analyses made on 17 grains from the hornblende-clinozoisite gneiss give  $^{206}\text{Pb}/^{238}\text{U}$  ages ranging from c. 110.6 Ma to 369.1 Ma, this spread of age data used very small proportion of the two minute LA-ICP-MS analysis signal in order to make it concordant. The weighted mean for the 14 grains is  $136.20 \pm 1.70$  Ma ( $2\sigma$ ) with a high MSWD of 4.10 suggesting this is not a single population (Figure 21). The same 14 grains also give a concordia age of  $139.90 \pm 1.3$  Ma but with a high MSWD of 0.59 ( $2\sigma$ ) (Figure 22D). As can be seen in Figure 22 there are also concordant ages  $> 250$  Ma. This indicates the  $136.20 \pm 1.70$  Ma age is likely an under estimation and can be regarded as a minimum age of crystallisation. The smear of ages lacking a flat region on the weighted mean plot suggests Pb-loss or partial recrystallization to varying degrees in all grains. CL images show no consistent correlation in internal structures to  $^{206}\text{Pb}/^{238}\text{U}$  ages. A Chi-square value of 0.000028 which is  $< 95\%$  confidence suggests some uncertainty in the age given by this sample and as a result is not considered geologically meaningful (Figure 21).

### Metre-scale thrust shear zone – PV1336B

Zircons from the m-scale thrust shear zone lack well-formed crystal faces and have varied morphologies ranging from rounded to irregular (Figure 20E). Internal structures range from faint oscillatory zoning, faint sector zoning and homogeneous centres in CL images. U-Pb analyses made on 22 grains from the m-scale thrust shear zone give  $^{206}\text{Pb}/^{238}\text{U}$  ages ranging from c. 106.2 Ma to 131 Ma, this spread of concordant age data used large proportion of the two minute LA-ICP-MS analysis signal. The weighted mean for all 22 grains is  $122.90 \pm 0.33$  Ma ( $2\sigma$ ) with a very high MSWD of 10.0 suggesting this is not a single population (Figure 21). The same 22 grains also give a concordia age of  $121.75 \pm 0.31$  Ma but with a low MSWD of 0.33 ( $2\sigma$ ) (Figure 22A). This indicates the  $122.90 \pm 0.33$  age is likely an under estimation and can be regarded as a minimum age of crystallisation. The smear of ages lacking a flat region on the weighted mean plot suggests Pb-loss or partial recrystallization to varying degrees in all grains. CL images show no consistent correlation in internal structures to  $^{206}\text{Pb}/^{238}\text{U}$  ages. Chi-square value of 0.00 which is  $<< 95\%$  confidence suggests some uncertainty in the age given by this sample and as a result is not considered geologically meaningful (Figure 21).

### Steeply dipping high strain zone – PV1702C1

Zircons from the steeply dipping high strain zone lack well-formed crystal faces and varied morphologies ranging from rounded to irregular (Figure 20C). Internal structures range from sector, oscillatory, planar to homogenous in CL images. 24 U-Pb analyses made on 27 grains from the steeply dipping high strain zone (PV1702C1) give  $^{206}\text{Pb}/^{238}\text{U}$  ages ranging from c. 96.8 Ma to 145.5 Ma, this spread of age data used very small proportion of the two minute LA-ICP-MS analysis signal in order to make it concordant. The weighted mean for the 24 grains is  $126.41 \pm 0.58$  Ma ( $2\sigma$ ) with a high MSWD of 10.0 suggesting this is not a single population (Figure 21). The same 24 grains also give a concordia age of  $127.95 \pm 0.54$  Ma but with a low MSWD of 0.33 ( $2\sigma$ ) (Figure 22F). This indicates the  $127.95 \pm 0.54$  age is likely an under estimation and can be regarded as a minimum age of crystallisation. The smear of ages lacking a flat region on the weighted mean plot suggest Pb-loss or partial recrystallization to varying degrees in all grains. CL images show no consistent correlation in internal structures to  $^{206}\text{Pb}/^{238}\text{U}$  ages. The Chi-square value of 0 which is  $\ll 95\%$  confidence suggests that the age given by this sample is also unreliable (Figure 21).

### Cumulative Probability Plots

Cumulative probability plots indicate that there is very little spread across the ages for all samples analysed. The weakly modified two-pyroxene - plagioclase gneiss (PV1232) and the trondhjemitic dyke (PV1234D) do not show any skew to the data and have normal distributions (Figure 23A). The m – scale thrust shear zone (PV1336) again does not show any skew to the data (Figure 23B). The hornblende-clinzoisite-plagioclase gneiss (PV1703) has two distinct peaks centred around 122 Ma and 138 Ma. The steeply dipping high strain zone (PV1702C1) has a single peak that is skewed towards the 135 Ma age (Figure 23C). The amphibole-clinzoisite gneiss (PV1708) shows a peak at 130–135 Ma and is skewed to this age (Figure 23C).

### Trace Element Patterns

Zircons from the Pembroke Granulite have steep, chondrite-normalised REE profiles, enriched in heavy rare earth element (HREE) contents relative to light rare earth element (LREE) contents (Figure 23). The only sample to demonstrate a lower HREE pattern compared to the LREE is the m – scale thrust shear zone (PV1336) (Figure 23B). All analyses exhibit positive Ce anomalies and most samples show a negative Eu anomaly. In all samples, there are 2–6 zircon grains that demonstrate a smaller weakly negative Eu anomaly when compared to the rest of the analyses within each sample (Figures 23 & 24). The zircons from the m – scale thrust shear zone, all show a

very weakly negative Eu anomaly followed by the trondhjemitic dyke samples (Figures 23 & 24). The strongest negative Eu anomaly comes from the hornblende-clinozoisite-plagioclase gneiss (PV1703) sample ( $Eu^* = 0.1189$ ,  $Sm/Eu = 3.892$ ) (Figure 24).

Yttrium (Y) content is positively correlated with Eu in several of the samples, with the host weakly modified two-pyroxene-plagioclase gneiss (PV1232) ( $R^2 = 0.9409$ ) and steeply dipping high stain zone (PV1702C1) ( $R^2 = 0.9229$ ) samples, having the closest relationship (Figure 25). The m – scale thrust shear zone (PV1336) ( $R^2 = 0.8148$ ), hornblende-clinozoisite-plagioclase gneiss (PV1703B) ( $R^2 = 0.8306$ ) and amphibole-clinozoisite gneiss (PV1708) ( $R^2 = 0.8405$ ) samples also demonstrate a close relationship between Y and Eu although there is more variation in the correlation (Figure 25). There is one sample that shows little to no correlation between Y and Eu, this is the trondhjemitic dyke (PV1234D) ( $R^2 = 0.2622$ ) (Figure 25). With the m – scale thrust shear zone, and trondhjemitic dyke tend to be more depleted in Y compared to the other samples.

In each method of analysis (U/Pb age dating, CL imaging and trace elements) there were some zircon grains that behaved in a different manner to the rest of the sample. In each sample, these grains were investigated further to see if there was any distinct pattern that was causing these grains to be different. Zircon grains that are younger than 120 My do not show any correlation to odd REE patterns,  $Eu^*$  anomalies, Y values or CL patterns. The same process was applied to the grains that have a flatter Eu anomaly (Figure 30) and again no discernible pattern was found, with the identified grains being from a range of ages, having variable  $Eu^*$  values, variable Y values and no consistent patterns in CL images.

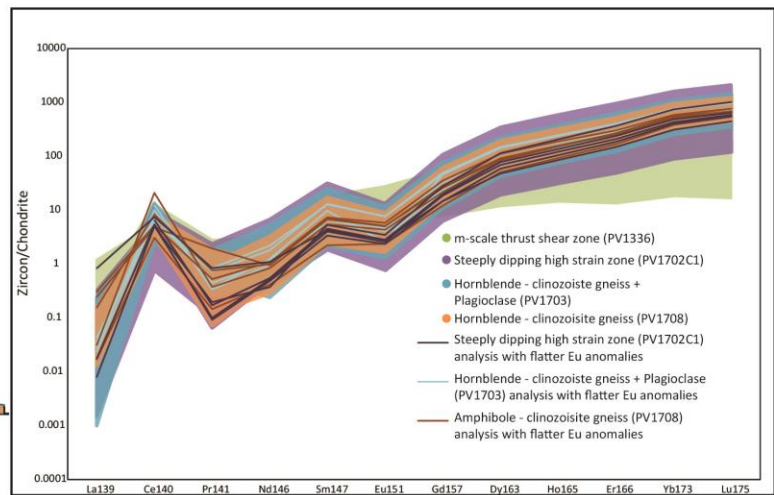
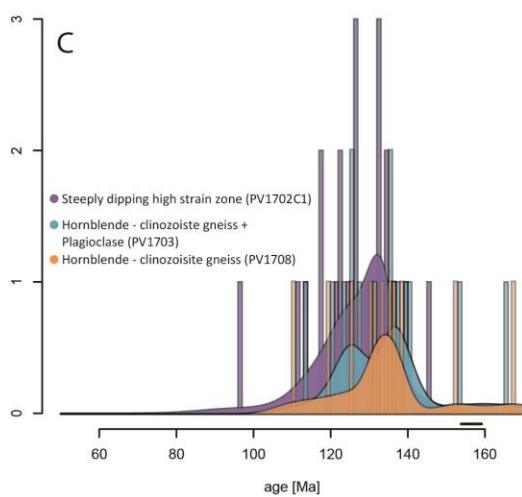
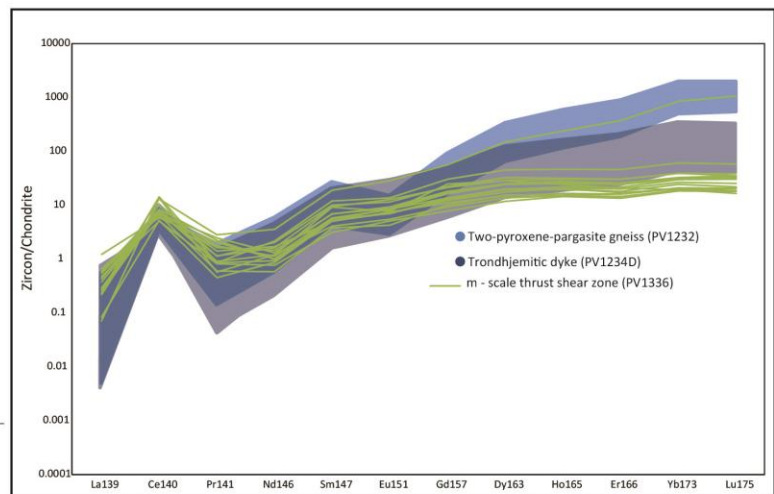
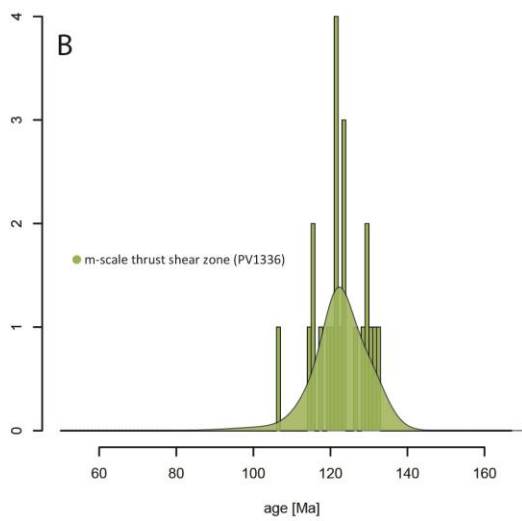
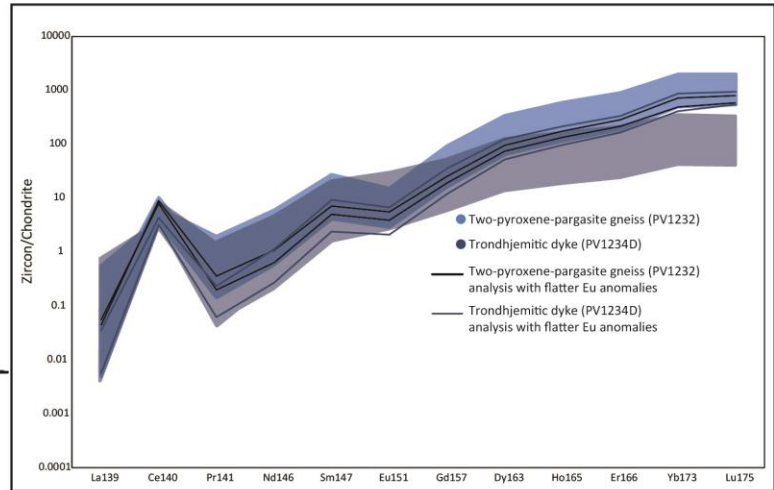
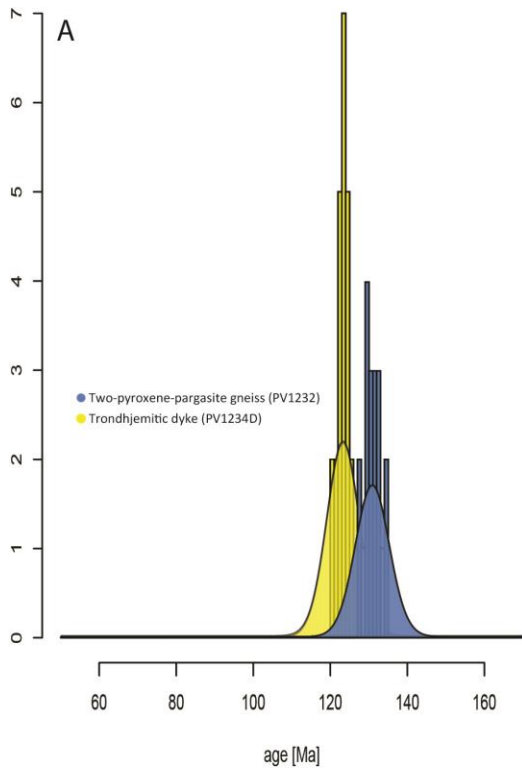
**Figure 23** - Chondrite-normalised REE plots and cumulative probability plots.

**A** – Two-pyroxene-plagioclase gneiss (PV1232), garnet reaction zone (PV1234GRZ) and trondhjemitic dyke (PV1234D). Modified from Elliot, 2016 (Figure 5 & 7)

**B** – m-scale thrust shear zone (PV1336) relative to trondhjemitic dyke, two-pyroxene - plagioclase gneiss and garnet reaction zone. Modified from Elliot, 2016 (Figure 5 & 7)

**C** – Steeply dipping high stain zone (PV1702C1), hornblende – clinozoisite gneiss + plagioclase (PV1703) and hornblende – clinozoisite gneiss (PV1708) relative to m-scale shear zone





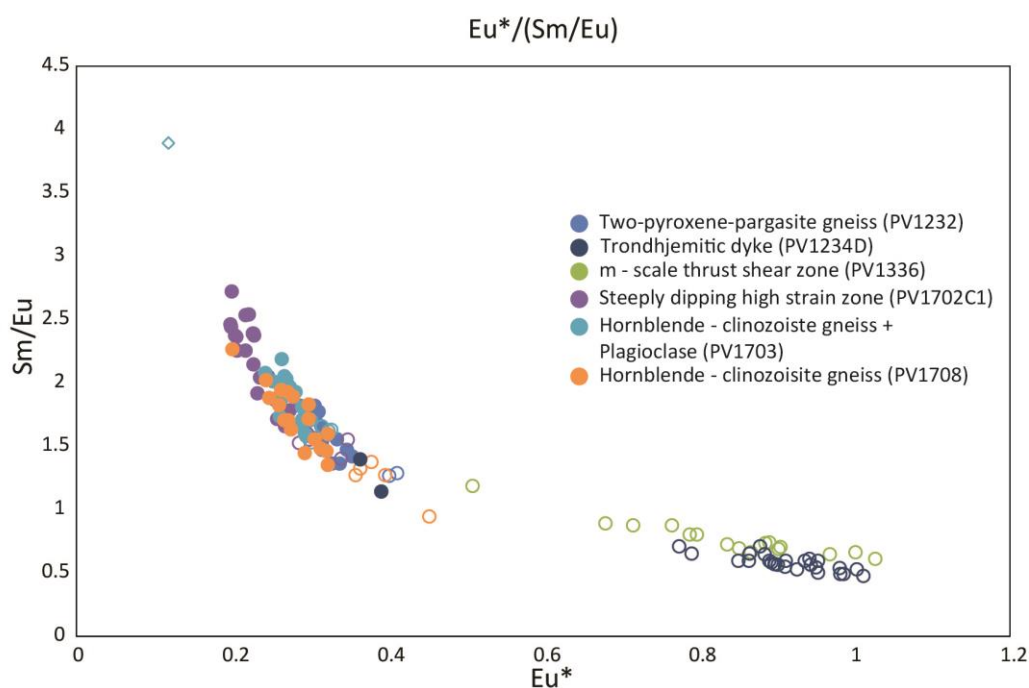


**Figure 24** - Eu anomaly ( $= \text{Eu}/\sqrt{\text{SmGd}}$ ) (Taylor and McLennan, 1986) vs Gd/Lu  
Open circles represent analysis with a flatter Eu anomaly  
Diamond represents the one grain with an abnormally high negative Eu anomaly

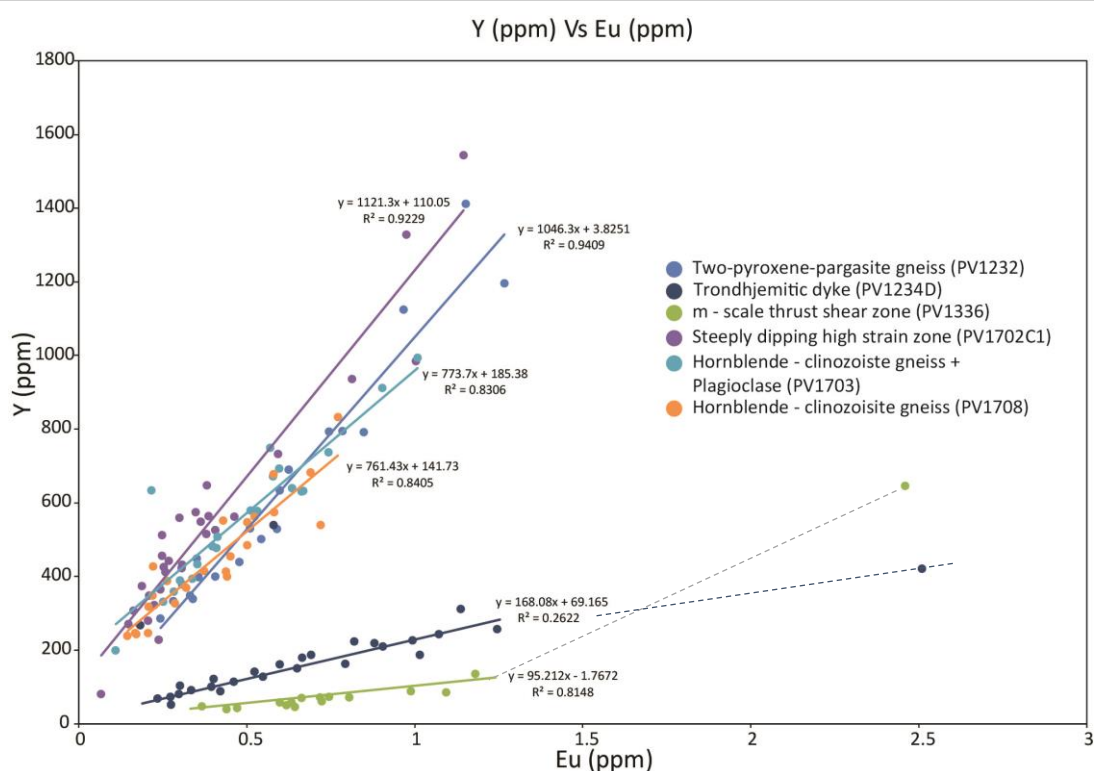


**Figure 25** - Y (ppm) Vs Eu (ppm) – Solid lines show compositional trends in Y and Eu in zircons for two-pyroxene-plagioclase gneiss (PV1232), garnet reaction zone (PV1234GRZ), trondhjemitic dyke (PV1234D), m-scale thrust shear zone (PV1336), steeply dipping high strain zone (PV1702C1), hornblende-clinozoisite gneiss + plagioclase (PV1703) and hornblende-clinozoisite gneiss (PV1708). Modified from Elliot, 2016 (Figure 8)



## Discussion

The Pembroke Valley has had extensive study by the likes of Blattner (1976); Blattner (2005); Clarke et al. (2005); Clarke et al. (2000); Daczko et al. (2001a); Daczko and Halpin (2009); Daczko et al. (2016); Hollis et al. (2003); Stowell et al. (2010); Stuart et al. (2016); Stuart et al. (2017, 2018b). However, these have focused on relationships lower in the valley, while the rocks studied here are at one of the highest safely accessible sections.

Granulite facies gabbroic gneiss (two-pyroxene–plagioclase  $\pm$  hornblende) that is cut by a spectacular grid of thin plagioclase-rich dykes with garnet reaction zones (Figure 6A) is deformed by numerous, variably-oriented, high strain zones in the Pembroke Valley, Fiordland, New Zealand (Daczko et al., 2001a; Daczko et al., 2016; Stuart et al., 2016; Stuart et al., 2017 and this study). A new steeply dipping high strain zone was examined for this thesis in the upper reaches of the Pembroke Valley. The microstructure of samples within and immediately surrounding the examined steeply dipping high strain zone are first used to argue for melt-present deformation. The melt is inferred to be externally-derived, reactive, and to have migrated through the steeply dipping high strain zone in a type of deformation-assisted reactive flow on the basis of a comparison of variably strained rocks, linked to changes in mineral assemblage and mineral modes as discussed below.

Zircon is carefully studied from one high and two intermediate strain samples and these results are compared to previously analysed zircon (Elliot, 2016) from (1) the precursor gabbroic gneiss, (2) a plagioclase-rich dyke, representative of those associated with garnet reaction zones, and (3) a thrust high strain zone. Together, these studies are used to examine the effects of melt migration through high strain zones on zircon modification. Modification of protolith zircon in the steeply dipping high strain zone examined in this study is characterised. These results are contrasted with the introduction of zircon xenocrysts to the m – scale thrust shear zone studied by Elliot (2016).

### **Microstructural criteria for recognising the former presence of melt in and immediately surrounding high strain zones**

Pseudomorphs of melt-filled pores are common microstructural criteria indicative of the former presence of melt in high-grade, metamorphic rocks (Brown, 2010; Holness and Sawyer, 2008; Sawyer, 1999; Vernon, 2011). These pseudomorphs are generally felsic in composition and represent the last stages of melt crystallisation, as the temperature dropped below the solidus (Levine et al., 2013; Rosenberg and Riller, 2000; Stuart et al., 2018b). However, pseudomorphs can

Page | 42

be more mafic in some examples (e.g. clinopyroxene in gabbro) (Holness and Sawyer, 2008). These melt pseudomorphs are described as being single or multiple minerals that now occupy the location of the inferred former melt pockets, i.e. the melt pseudomorphs have a different composition to that of the former melt. There are five different microstructures that have been identified in this thesis that indicate the former presence of melt in variably strained rocks of the Pembroke Granulite. These microstructures are expanded upon below and are not the only ones that can be used to indicate the former presence of melt and supplementary indicative microstructures are discussed by Sawyer (1999); Vernon (2011) and can be found in other examples of rocks formed by melt-present deformation in the Pembroke Granulite and elsewhere in the world (Stuart et al., 2018b).

#### Small ( $\leq 60^\circ$ ) dihedral angles of interstitial grains

Dihedral angles of  $60^\circ$  or less where one grain meets two other grains are used as evidence for former melt within rocks (Holness, 2006; Vernon, 2011). The part of the grain forming the small dihedral angle is interpreted as a pseudomorph of melt. These angles are distinctly smaller ( $<60^\circ$ ) than those that involve the same minerals in melt-free high-grade metamorphic rocks ( $>100^\circ$ ) (Beere, 1975; Hasalová et al., 2008; Holness, 2006; Holness and Sawyer, 2008; Rosenberg and Riller, 2000; Stuart et al., 2018b; Vernon, 2011). These angles represent a threshold at which melt spreads along grain edges forming a continuous network of channels through which melt may move if of low enough viscosity (Vernon, 2011). Examples from Holness and Sawyer (2008); Levine et al. (2013); Stuart et al. (2018b); Vernon (2011) and others present felsic minerals as melt pseudomorphs, with quartz being the main pseudomorphs in plagioclase rich rocks and plagioclase being the main pseudomorphs in quartz rich rocks. However, in this study there is very little to no quartz in the rocks, with plagioclase being the main pseudomorph of the melt (e.g. Figure 14.2, 15.3, 16.2, 17.3 & 19.2). There are also other minerals that have pseudomorphed the melt besides the plagioclase and include: rutile (Figure 15.5), apatite (Figure 14.3) and clinozoisite (Figure 15.1 & 16.1). Due to polished thin sections being two-dimensional slices through three-dimensional mineral crystals, the measured dihedral in these sections are only apparent angles and are not necessarily true dihedral angles. In thin sections that are not perpendicular to grain boundaries, dihedral angles can appear to be smaller than they actually are (Vernon, 2011). Therefore, simple inspection of interfacial angles in a thin section can be misleading. However, the very low apparent dihedral angles identified in this study are convincing evidence for the former presence of melt.

### **Veinlets and elongate interstitial grains**

Films or veinlets of inferred former melt that have been pseudomorphed by plagioclase (Figure 15.2, 15.4, 16.5, 16.6, 17.2, 18.6, 19.3 & 19.8) or clinozoisite (Figure 15.1) are not necessarily reliable criteria for the former presence of melt during deformation. However, their formation is consistent with the former presence of melt and may be supported by the identification of the other criteria presented here (Rosenberg and Riller, 2000; Sawyer, 1999; Stuart et al., 2018b; Vernon, 2011). Melt films have been produced in melting experiments by Laporte (1994). These melt films and veinlets were found at grain triple boundaries with low dihedral angles ( $<60^\circ$ ), where the melt spread along the adjacent grain boundaries. These pseudomorphs of melt are commonly observed in small-scale faults or veins, where they are interpreted as the last leucosome to form (Sawyer, 2001; Stuart et al., 2016; Stuart et al., 2018b). This is due to an overpressure in a high strain zone causing the remaining fluids to be pushed through more ductile regions of the system into lower strain zones which will eventually exhaust the fluid in the high strain zones causing a drop-in pressure allowing the high strain zone to solidify fully.

### **Melt pseudomorphs**

Holness and Sawyer (2008) found that melt, pseudomorphed predominantly by non-twinned K-feldspar, with minor amounts of quartz, is concentrated in films and pools around reactant biotite grains. In this study single-mineral feldspar pseudomorphs of biotite (Figure 15.7 & 16.6) have been found; plagioclase has also been found pseudomorphing amphibole and clinozoisite (Figure 18.8). As the plagioclase is adjacent to biotite, these replacement textures most likely represent a propagating reaction front (Holness and Sawyer, 2008). The compositions of the pseudomorphs are unlikely to represent the last composition of the melt in the pore space. The textures and pseudomorphs described above are indicative of mass transfer at a grain scale (Holness and Sawyer, 2008).

### **Cusped grains**

The former presence of melt in now melt-poor rocks has been inferred from the presence of highly cusped grains with low dihedral angles (Harte et al., 1991; Holness and Sawyer, 2008; Marchildon and Brown, 2002; Rosenberg and Riller, 2000; Sawyer, 1999; Sawyer, 2001; Vernon, 2011). It is inferred that these textures represent former melt that has partially penetrated along grain boundaries. Using BSE imaging, Rosenberg and Riller (2000) observed interstitial pockets of plagioclase having concave outward curvatures, at quartz junctions in statically recrystallized, partly melted granite. Similar shapes with extensions (thought to be low dihedral angles) were also found by Holness and Clemens (1999) these extensions occurred in between two solid grain

boundaries. Cuspate areas in this study typically involve plagioclase as the melt pseudomorph and amphibole as the solid phase that is being infilled (Figure 14.4, 15.6, 17.4, 18.2 & 19.6). These cuspate shapes can result from partial inclusions of one mineral into another, formed during growth of metamorphic minerals in the absence of melt (e.g. Vernon (2011) Figure 4 & 5), due to mutual interference of simultaneously growing primary grains, possibly aided by some later solid-state deformation. Thus, care is needed while using this criteria and should only be used if samples demonstrate other indicators for the former presence of melt or the boundaries of the cuspate grains appear to taper into small, dihedral angles.

### Symplectites

Symplectite is a term applied to fine-grained intergrowths resulting from the combined growth of two or more minerals as they replace another mineral. Symplectites may form by reactions between peritectic grains and cooling melt, thus are a good indicator of the former presence of melt (Vernon, 2011; Winter, 2014). This replacement may be partial or complete where the original mineral has been pseudomorphed by the symplectite. Symplectic mineral aggregates are common in the low-strain weakly modified two-pyroxene gneiss (PV1701B). These assemblages show no evidence for internal modification or deformation during melt-rock interaction. They most likely formed under static conditions, due to melt-rock interactions by diffuse porous flow along grain boundaries (Stuart et al., 2016; Stuart et al., 2017). Comparatively these structures are rare in the intermediate and high strain samples. Daczko et al. (2016); Stuart et al. (2016); Stuart et al. (2017) and Lee et al. (2018) all show that under dynamic conditions these symplectite assemblages do not occur.

## Petrology

Variably strained samples described in this thesis include low-strain weakly modified two-pyroxene gneiss, intermediate strain hornblende–clinozoisite gneiss and high strain clinozoisite amphibolite (Figure 7B shows these relationships). With increasing strain, the degree of modification in mineral assemblage and modal abundance also increases in both domains of the modified precursor rocks (gabbroic gneiss (two-pyroxene–plagioclase  $\pm$  hornblende)) and garnet reaction zones) (Figure 12). An increase in amphibole, clinozoisite and to a lesser extent garnet is observed with a decrease in the abundance of plagioclase. The variations are inferred to be linked to the volume of time-integrated melt migration and potentially to variations in melt chemistry. Stuart et al. (2016); Stuart et al. (2018a) add to this interpretation, presenting a model involving melt migration through high strain zones in the Pembroke Valley which results in changes to the



bulk rock chemistry, directly related to the amount and type of melt migrating through the high strain zone. Stuart et al. (2016); Stuart et al. (2018a) imply that little to no melt stagnated and crystallized in high strain zones, instead invoking a model of melt flux where most of the melt passed through the mostly solid high strain zone.

## **Melt-present deformation effect on magmatic zircon**

### **Magmatic origin of zircon**

The origin of zircon grains from weakly modified two-pyroxene-plagioclase gneiss, hornblende – clinozoisite + plagioclase gneiss, hornblende – clinozoisite gneiss and the steeply dipping high strain zone examined in this study is most likely igneous. This is recognised by steep HREE patterns (Figure 23C), high Y (Figure 25), high Th/U, positive Ce anomalies and negative Eu anomalies (Hoskin and Schaltegger, 2003; Rubatto, 2002). The overall strong negative Eu anomalies (Figure 23C) likely reflect the preferential partitioning of  $\text{Eu}^{2+}$  into plagioclase during evolution of the original magma (Belousova et al., 2002; Rubatto, 2002). The range of ages for the weakly modified two-pyroxene-plagioclase gneiss, steeply dipping high strain zone, hornblende – clinozoisite + plagioclase gneiss and hornblende – clinozoisite gneiss (Figure 21 & 22) along with CL images (Figure 20) suggests that the zircon U-Pb systems have been modified to varying degrees, post igneous crystallisation. As discussed by Elliot (2016) and outlined above (microstructural criteria), this is possibly due to partial melt assisted diffuse porous melt flow. Diffuse metamorphic textures that overprint sectors, oscillatory and planar internal patterns (Figure 20) are inferred to be associated with modification of original magmatic zircon during this diffuse porous melt flow.

The concordia ages for weakly modified two-pyroxene-plagioclase gneiss ( $130.93 \pm 0.36$  Ma), whilst not all statistically accurate, can be regarded as a minimum age for magmatic emplacement of the Pembroke Granulite. A more tangible age of emplacement for the Pembroke Granulite is somewhat older, closer to the hornblende – clinozoisite gneiss age which are similar to the age suggested by Stowell et al. (2010) at around 134 Ma. Although, Stowell et al. (2010) were unsure as to whether this age signified igneous or metamorphic processes.

Zircon grains analysed by Elliot (2016), from a trondhjemitic dyke also indicate an igneous origin, showing oscillatory zoning, well-formed crystal faces, positive HREE slope (Figure 23A), positive Ce anomalies and negative Eu anomalies. The shallower Eu anomalies in the trondhjemitic dyke compared to those in the weakly modified two-pyroxene-plagioclase gneiss, high strain zone, hornblende – clinozoisite + plagioclase gneiss and amphibole – clinozoisite gneiss zircons suggest

less partitioning of  $\text{Eu}^{2+}$  into plagioclase during the magma evolution (Belousova et al., 2002), most likely due to diminished feldspar growth under high-grade metamorphic conditions (Rubatto, 2002) or a fundamental difference in magma composition. Patchy, metamorphic textures can be seen in these grains (Elliot, 2016) suggesting that the U/Pb system may have been partially modified. In the trondhjemitic dyke sample there is a flattening of HREE and depletion in Y, consistent with the growth of a HREE and Y enriched mineral such as garnet. Depletion of HREE and Y concentrations is commonly found to occur in zircon which has co-crystallised with garnet where the garnet preferentially uptakes HREE and Y when compared to zircon (Rubatto, 2002).

A m – scale thrust shear zone was analysed by Elliot (2016) who suggested that oscillatory zoning, lack of metamorphic overgrowths or patchy recrystallization structures and positive Ce anomalies are suggestive of slow magmatic crystallisation (Rubatto, 2002). This sample has very shallow Eu anomalies (Figure 23B), which are consistent with little to no plagioclase growth (Belousova et al., 2002), under the high-grade metamorphic conditions (<6 to <11 kbar and 650–850°C) found within the Pembroke Granulite (Stuart et al., 2017) or a fundamental difference in magma composition. The depletion of Y and HREEs and the strong linear relationship between Y and Eu (Figure 25), can be explained by crystallisation from melt which has been heavily fractionated by the growth of garnet (Rubatto, 2002). Whilst garnet growth is documented in the m-scale thrust shear zone (Daczko et al., 2001a) as a reaction product of melt-rock interaction (Stuart et al., 2017), the broad age range of individual grains suggests that they are most probably xenocrysts that have been transported by the fluxing melt and introduced into the rock.

#### Melt – present deformation

Chemically, there are two very distinct groups of zircon from the Pembroke Granulite, those with a low  $\text{Eu}^*$  and high Y values and those with high  $\text{Eu}^*$  and low Y values (Figure 24 & 25). Samples from the trondhjemitic dyke and m – scale thrust shear zone have chemically very similar patterns in terms of Y and  $\text{Eu}^*$ . This might suggest that these are related to each other and that the trondhjemitic dyke sample has been modified in the thrust shear zone. Although, that is where the similarities end, with the REE patterns (Figure 23B) showing that the m-scale thrust shear zone is depleted in HREE, when compared to the trondhjemitic dyke. A possible explanation for this is that the m-scale thrust shear zone has multiple events of melt flux through it. Each event is inferred to have picked up and carried zircon xenocrysts structurally higher up a system of high strain zones.

Comparatively, grains from the weakly modified two-pyroxene-plagioclase gneiss, hornblende – clinozoisite + plagioclase gneiss, hornblende – clinozoisite gneiss and steeply dipping high strain

zone examined in this study all have very similar REE, Y and Eu\* patterns (Figure 23, 24 & 25). Due to the consistent nature of the REE patterns across all these samples, this style of melt-present deformation has only weakly modified the zircon grains from their original composition, with most of this modification affecting the internal structure of the grains. Thus, it is likely the diffuse porous melt flow was Zr under saturated and caused small amounts of dissolution in the original zircons with limited or no new zircon growth.

The trondhjemitic dyke has a very typical igneous pattern to what is expected if zircon and garnet are crystallising simultaneously. Modified zircon due to melt assisted deformation has occurred in the hornblende – clinozoisite + plagioclase gneiss and hornblende – clinozoisite gneiss, not only affecting their internal morphology but also the spread of ages seen in both samples (discussed in the next section). The m – scale thrust shear zone saw the introduction of xenocryst zircons that have seen multiple stages of subsequent deformation altering their REE chemistry and morphologies. Whereas the zircons from the steeply dipping high strain zone just see the altering of morphologies by the fluxed melt (Figure 26).

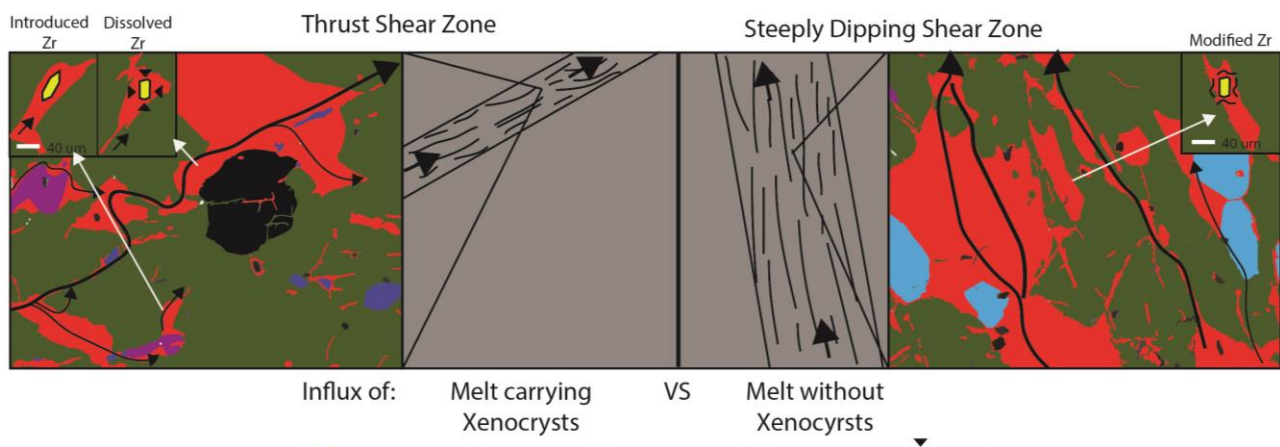


**Figure 26** – Model of zircon modification versus introduction

**Left** – m – scale thrust shear zone – showing that original magmatic zircon was dissolved by the flux of melt. This melt flux also introduced zircon xenocrysts from deeper in the system.

**Right** – Steeply dipping high strain zone – showing that in this area of the valley melt migration modified zircon grains without introducing xenocrysts or dissolving them entirely.

### Zircon data errors and variable interpretations

As can be seen in Figure 22, the weakly modified two-pyroxene-plagioclase gneiss, trondhjemitic dyke and m – scale thrust shear zone have very nicely defined concordia ages with a small error ellipse. Whereas the hornblende – clinozoisite + plagioclase gneiss, hornblende – clinozoisite

gneiss and steeply dipping high strain zone have larger error ellipse and a larger spread of individual grain ages. This increase in error is due to the proportion of each two minute signal integrated and then plotted on concordia plots in Figure 22. The plots with smaller error ellipses (figure 22 A, B & E) integrated a larger proportion of LA-ICP-MS analysis signal (i.e. > 1.5 minutes of the two minute analysis) when compared to the samples with larger error ellipses (Figure 22 C, D & F) which only used a very small fraction of concordant LA-ICP-MS signal (typically <30 seconds of the two minute signal).

As seen in the hornblende – clinozoisite + plagioclase gneiss, hornblende – clinozoisite gneiss and steeply dipping high strain zone samples, there is a large spread of ages including some old ‘inherited’ grains (>250 Ma), old grains (145 -160 Ma), young grains (129-139 Ma) and very young grains (<129 Ma) across these samples. This spread of age ranges fits into the currently accepted ages for key geological events within Fiordland and the Pembroke Valley. With the >250 Ma ages being partially inherited from the Broader Median Batholith, the 145-160 Ma grains either also being related to Median Batholith (Hollis et al., 2003) or Dioritic Orthogneiss along the eastern margin of the Arthur River Complex (Hollis et al., 2003; Stowell et al., 2010). The grains ranging from 129-139 Ma are thought to be the magmatic emplacement age of the Pembroke Granulite (Clarke et al., 2005; Daczko and Halpin, 2009; Hollis et al., 2003; Stowell et al., 2010; Stuart et al., 2016; Stuart et al., 2017, 2018b) while the very young grains <129 Ma are thought to be the last of the melt flux to occur in the valley (Stowell et al., 2010). In the example of the hornblende – clinozoisite gneiss which has the largest spread of age data, a granitoid melt, could be injected into already-emplaced mafic rock, with this melt carrying existing zircons (including inherited ones) and possibly crystallized new grains causing the spread of ages that is seen (Belousova et al., 2015). Alternatively, the age spread may be due to variable modification of a signal magmatic zircon population.

Granulite facies rocks frequently show a large spread in their zircon ages which raises important questions such as; can the dates be regarded as real, has the U-Pb isotope system been disturbed, and if so, how and under what conditions? (Ewing et al., 2013; Kunz et al., 2018; Vavra et al., 1999). If we consider zircon disturbance in granulite facies rocks as a potential answer to this age spread due to either 1) fluid-assisted modification of the zircon during metamorphism under granulite-facies conditions or 2) high temperature disturbance (>850°C), although no particular process has been accepted to account for this phenomenon (Ewing et al., 2013; Kunz et al., 2018; Roberts et al., 2018; Vavra et al., 1999). Then the ability to link and interpret the observed scatter



in these ages is seriously hampered. Leaving the real meaning behind the grain ages presented in this thesis and potentially through the region still open for interpretation. This still leaves the question of why are the hornblende – clinozoisite + plagioclase gneiss, hornblende – clinozoisite gneiss and high strain zone samples different to the weakly modified two-pyroxene-plagioclase gneiss, trondhjemitic dyke and m – scale thrust shear zone samples? In order to understand this, the P-T conditions of all samples would need to be analysed to determine if there is a correlation between T-P and samples interpreted to be disturbed.

## **Conclusion**

The modification that occurs when rocks partially melt has a profound effect on their morphological, textural and compositional evolution. At a micro scale, melt–rock interaction during melt-present deformation within the Pembroke Granulite is characterised by 1) microstructures indicative of the former presence of melt, (low dihedral angles, veinlets and elongate interstitial grains, melt pseudomorphs, cusped grains and symplectites), and 2) increased modes of amphibole and clinozoisite and decreased modes of plagioclase linked to the hydration of the precursor granulite rock. Melt-present deformation within the Pembroke Granulite is also linked to modification of zircon morphologies, trace element compositions and U-Pb data. With modification occurring due to the flux of a fluid that is likely Zr undersaturated or due to the introduction of zircon xenocrysts. There are shortfalls when it comes to interpretation of these results including; sampling bias, disturbance and multiple plausible histories for the region. In regions as young as the Pembroke Valley where the shear zones are not much younger than the host rock, and the error introduced by misinterpreting the age data is small. However if a much older rock (e.g. Archean in age) has had multiple episodes of melt flux and resetting of the U/Pb system in zircon then the range of error could be quite large with data suggesting much younger dates than is actually true. The microstructures and mineral chemistry of the Pembroke Granulite represent a unique example of pathways for efficient mass transfer through diffuse porous flow, assisted by melt present deformation in the lower crust. Thus, diffuse porous flow has the potential to be an important mechanism of mass transfer in the lower crust, affecting host rock microstructure and chemistry, along with modifying and introducing zircon. Caution must be applied when dating highgrade terrains and shear zones.

## Reference list

- Beach, A., and Fyfe, W., 1972, Fluid transport and shear zones at Scourie, Sutherland: Evidence of overthrusting?: *Contributions to Mineralogy and Petrology*, v. 36, no. 3, p. 175-180.
- Beere, W., 1975, A unifying theory of the stability of penetrating liquid phases and sintering pores: *Acta Metallurgica*, v. 23, no. 1, p. 131-138.
- Belousova, E., Griffin, W., O'Reilly, S. Y., and Fisher, N., 2002, Igneous zircon: trace element composition as an indicator of source rock type: *Contributions to Mineralogy and Petrology*, v. 143, no. 5, p. 602-622.
- Belousova, E. A., Jimenez, J. M. G., Graham, I., Griffin, W. L., O'Reilly, S. Y., Pearson, N., Martin, L., Craven, S., and Talavera, C., 2015, The enigma of crustal zircons in upper-mantle rocks: clues from the Tumut ophiolite, southeast Australia.: *Geology*, v. 43, no. 2, p. 119-122.
- Blattner, 1976, Replacement of hornblende by garnet in granulite facies assemblages near Milford Sound, New Zealand: *Contributions to Mineralogy and Petrology*, v. 55, no. 2, p. 181-190.
- Blattner, P., 2005, Transport of low-aH<sub>2</sub>O dehydration products to melt sites via reaction-zone networks, Milford Sound, New Zealand: *Journal of Metamorphic Geology*, v. 23, no. 7, p. 569-578.
- Bradshaw, J. Y., 1990, Geology of crystalline rocks of northern Fiordland: Details of the granulite facies Western Fiordland Orthogneiss and associated rock units: *New Zealand Journal of Geology and Geophysics*, v. 33, no. 3, p. 465-484.
- Breton, N. L., and Thompson, A. B., 1988, Fluid-absent (dehydration) melting of biotite in metapelites in the early stages of crustal anatexis: *Contributions to Mineralogy and Petrology*, v. 99, no. 2, p. 226-237.
- Brown, M., 2004, The mechanism of melt extraction from lower continental crust of orogens: *Trans. R. Soc. Edinb.-Earth Sci.*, v. 95, p. 35-48.
- Brown, M., 2010, Melting of the continental crust during orogenesis: the thermal, rheological, and compositional consequences of melt transport from lower to upper continental crust This article is one of a selection of papers published in this Special Issue on the theme Lithoprobe—parameters, processes, and the evolution of a continent: *Canadian Journal of Earth Sciences*, v. 47, no. 5, p. 655-694.
- Cartwright, I., and Barnicoat, A. C., 2003, Geochemical and stable isotope resetting in shear zones from Täschalp: constraints on fluid flow during exhumation in the Western Alps: *Journal of Metamorphic Geology*, v. 21, no. 2, p. 143-161.
- Clarke, G. L., Daczko, N. R., Klepeis, K. A., and Rushmer, T., 2005, Roles for fluid and/or melt advection in forming high-P mafic migmatites, Fiordland, New Zealand: *Journal of Metamorphic Geology*, v. 23, no. 7, p. 557-567.
- Clarke, G. L., Klepeis, K. A., and Daczko, N. R., 2000, Cretaceous high- P granulites at Milford Sound, New Zealand: metamorphic history and emplacement in a convergent margin setting: *Journal of Metamorphic Geology*, v. 18, no. 4, p. 359-374.
- Clemens, J. D., and Vielzeuf, D., 1987, Constraints on melting and magma production in the crust: *Earth and Planetary Science Letters*, v. 86, no. 2, p. 287-306.
- Corfu, F., Hanchar, J. M., Hoskin, P. W. O., and Kinny, P., 2003, Atlas of Zircon Textures: Reviews in Mineralogy and Geochemistry, v. 53, no. 1, p. 469-500.
- Daczko, N. R., Clarke, G. L., and Klepeis, K. A., 2001a, Transformation of two-pyroxene hornblende granulite to garnet granulite involving simultaneous melting and fracturing of the lower crust, Fiordland, New Zealand: *Journal of Metamorphic Geology*, v. 19, no. 5, p. 549-562.
- Daczko, N. R., and Halpin, J. A., 2009, Evidence for melt migration enhancing recrystallization of metastable assemblages in mafic lower crust, Fiordland, New Zealand: *Journal of Metamorphic Geology*, v. 27, no. 2, p. 167-185.

- Daczko, N. R., Klepeis, K. A., and Clarke, G. L., 2001b, Evidence of Early Cretaceous collisional-style orogenesis in northern Fiordland, New Zealand and its effects on the evolution of the lower crust: *Journal of Structural Geology*, v. 23, no. 4, p. 693-713.
- Daczko, N. R., Piazzolo, S., Meek, U., Stuart, C. A., and Elliott, V., 2016, Hornblende delineates zones of mass transfer through the lower crust: *Sci Rep*, v. 6, p. 31369.
- Delaney, P. T., and Pollard, D. D., 1981, Deformation of host rocks and flow of magma during growth of minette dikes and breccia-bearing intrusions near Ship Rock, New Mexico: U.S. Geological Survey Professional Papers, v. 1202, p. <xocs:firstpage xmlns:xocs=""/>.
- Delaney, P. T., and Pollard, D. D., 1982, Solidification of basaltic magma during flow in a dike: *American Journal of Science*, v. 282, no. 6, p. 856-885.
- Elhlou, S., Belousova, E., Griffin, W., Pearson, N. J., and O'Reilly, S., 2006, Trace element and isotopic composition of GJ red zircon standard by Laser Ablation.
- Ewing, T. A., Hermann, J., and Rubatto, D., 2013, The robustness of the Zr-in-rutile and Ti-in-zircon thermometers during high-temperature metamorphism (Ivrea-Verbano Zone, northern Italy): *Contributions to Mineralogy and Petrology*, v. 165, no. 4, p. 757-779.
- Harte, B., Pattison, D. R. M., and Linklater, C. M., 1991, Field Relations and Petrography of Partially Melted Pelitic and Semi-Pelitic Rocks, *in* Voll, G., Töpel, J., Pattison, D. R. M., and Seifert, F., eds., *Equilibrium and Kinetics in Contact Metamorphism: The Ballachulish Igneous Complex and Its Aureole*: Berlin, Heidelberg, Springer Berlin Heidelberg, p. 181-209.
- Hasalová, P., Schulmann, K., Lexa, O., Štípská, P., Hrouda, F., Ulrich, S., Haloda, J., and Týcová, P., 2008, Origin of migmatites by deformation-enhanced melt infiltration of orthogneiss: a new model based on quantitative microstructural analysis: *Journal of Metamorphic Geology*, v. 26, no. 1, p. 29-53.
- Hollis, J. A., Clarke, G. L., Klepeis, K. A., Daczko, N. R., and Ireland, T. R., 2003, Geochronology and geochemistry of high-pressure granulites of the Arthur River Complex, Fiordland, New Zealand: Cretaceous magmatism and metamorphism on the palaeo-Pacific Margin: *Journal of Metamorphic Geology*, v. 21, no. 3, p. 299-313.
- Holness, 2006, Melt–Solid Dihedral Angles of Common Minerals in Natural Rocks: *Journal of Petrology*, v. 47, no. 4, p. 791-800.
- Holness, and Sawyer, 2008, On the Pseudomorphing of Melt-filled Pores During the Crystallization of Migmatites: *Journal of Petrology*, v. 49, no. 7, p. 1343-1363.
- Holness, M. B., and Clemens, J. D., 1999, Partial melting of the Appin Quartzite driven by fracture-controlled H<sub>2</sub>O infiltration in the aureole of the Ballachulish Igneous Complex, Scottish Highlands: *Contributions to Mineralogy and Petrology*, v. 136, no. 1, p. 154-168.
- Hoskin, P. W. O., and Schaltegger, U., 2003, The composition of zircon and igneous and metamorphic petrogenesis: *Reviews in Mineralogy and Geochemistry*, v. 53, p. <xocs:firstpage xmlns:xocs=""/>.
- Jackson, S. E., Pearson, N. J., Griffin, W. L., and Belousova, E. A., 2004, The application of laser ablation-inductively coupled plasma-mass spectrometry to in situ U–Pb zircon geochronology: *Chemical Geology*, v. 211, no. 1, p. 47-69.
- Jochum, K. P., Weis, U., Schwager, B., Stoll, B., Wilson, S. A., Haug, G. H., Andreae, M. O., and Enzweiler, J., 2016, Reference Values Following ISO Guidelines for Frequently Requested Rock Reference Materials: *Geostandards and Geoanalytical Research*, v. 40, no. 3, p. 333-350.
- Kunz, B. E., Regis, D., and Engi, M., 2018, Zircon ages in granulite facies rocks: decoupling from geochemistry above 850 °C?: *Contributions to Mineralogy and Petrology*, v. 173, no. 3, p. 26.
- Landis, C. A., and Coombs, D. S., 1967, Metamorphic belts and orogenesis in southern New Zealand: *Tectonophysics*, v. 4, no. 4, p. 501-518.

- Langone, A., and Tiepolo, M., 2015, U-Th-Pb "multi-phase" approach to the study of crystalline basement: Application to the northernmost sector of the Ivrea-Verbano Zone (Alps): *Periodico di Mineralogia*, v. 84, no. 3B, p. <xocs:firstpage xmlns:xocs=""/>.
- Laporte, D., 1994, Wetting behavior of partial melts during crustal anatexis: the distribution of hydrous silicic melts in polycrystalline aggregates of quartz: *Contributions to Mineralogy and Petrology*, v. 116, no. 4, p. 486-499.
- Lee, A. L., Torvela, T., Lloyd, G. E., and Walker, A. M., 2018, Melt organisation and strain partitioning in the lower crust: *Journal of Structural Geology*, v. 113, p. 188-199.
- Levine, J. S. F., Mosher, S., and Siddoway, C. S., 2013, Relationship between syndeformational partial melting and crustal-scale magmatism and tectonism across the Wet Mountains, central Colorado: *Lithosphere*, v. 5, no. 5, p. 456-476.
- Maaløe, S., 1982, Geochemical aspects of permeability controlled partial melting and fractional crystallization: *Geochimica et Cosmochimica Acta*, v. 46, no. 1, p. 43-57.
- Marchildon, N., and Brown, M., 2002, Grain-scale melt distribution in two contact aureole rocks: implications for controls on melt localization and deformation: *Journal of Metamorphic Geology*, v. 20, no. 4, p. 381-396.
- Mortimer, N., Tulloch, A. J., Spark, R. N., Walker, N. W., Ladley, E., Allibone, A., and Kimbrough, D. L., 1999, Overview of the Median Batholith, New Zealand: a new interpretation of the geology of the Median Tectonic Zone and adjacent rocks: *Journal of African Earth Sciences*, v. 29, no. 1, p. 257-268.
- Phipps Morgan, J., and Holtzman, B. K., 2005, Vug waves: A mechanism for coupled rock deformation and fluid migration: *Geochemistry, Geophysics, Geosystems*, v. 6, no. 8, p. n/a-n/a.
- Pollard, D. D., 1973, Derivation and evaluation of a mechanical model for sheet intrusions: *Tectonophysics*, v. 19, no. 3, p. 233-269.
- Roberts, N. M. W., Yang, Q.-Y., and Santosh, M., 2018, Rapid oxygen diffusion during high temperature alteration of zircon: *Scientific Reports*, v. 8, no. 1, p. 3661.
- Rosenberg, C. L., and Riller, U., 2000, Partial-melt topology in statically and dynamically recrystallized granite: *Geology*, v. 28, no. 1, p. 7-10.
- Rubatto, D., 2002, Zircon trace element geochemistry: partitioning with garnet and the link between U-Pb ages and metamorphism: *Chemical Geology*, v. 184, no. 1, p. 123-138.
- Sawyer, 1999, Criteria for the recognition of partial melting: *Physics and Chemistry of the Earth, Part A: Solid Earth and Geodesy*, v. 24, no. 3, p. 269-279.
- Sawyer, E. W., 2001, Melt segregation in the continental crust: distribution and movement of melt in anatectic rocks: *Journal of Metamorphic Geology*, v. 19, no. 3, p. 291-309.
- Secor, D. T., Jr., and Pollard, D. D., 1975, On the stability of open hydraulic fractures in the Earth's crust: *Geophysical Research Letters*, v. 2, no. 11, p. 510-513.
- Sleep, N. H., 1988, Tapping of melt by veins and dikes: *Journal of Geophysical Research: Solid Earth*, v. 93, no. B9, p. 10255-10272.
- Spence, D. A., Sharp, P. W., and Turcotte, D. L., 1987, Buoyancy-driven crack propagation: a mechanism for magma migration: *J. Fluid Mech.*, v. 174, no. -1, p. 135-153.
- Stevenson, J. A., Daczko, N. R., Clarke, G. L., Pearson, N., and Klepeis, K. A., 2005, Direct observation of adakite melts generated in the lower continental crust, Fiordland, New Zealand: *Terra Nova*, v. 17, no. 1, p. 73-79.
- Stowell, H., Parker, K. O., Gatewood, M., Tulloch, A., and Koenig, A., 2014, Temporal links between pluton emplacement, garnet granulite metamorphism, partial melting and extensional collapse in the lower crust of a Cretaceous magmatic arc, Fiordland, New Zealand: *Journal of Metamorphic Geology*, v. 32, no. 2, p. 151-175.



- Stowell, H., Tulloch, A., Zuluaga, C., and Koenig, A., 2010, Timing and duration of garnet granulite metamorphism in magmatic arc crust, Fiordland, New Zealand: *Chemical Geology*, v. 273, no. 1, p. 91-110.
- Stuart, C. A., Daczko, N. R., and Piazzolo, S., 2016, Local partial melting of the lower crust triggered by hydration through melt–rock interaction: an example from Fiordland, New Zealand: *Journal of Metamorphic Geology*, v. 35, no. 2, p. 213-230.
- Stuart, C. A., Piazzolo, S., and Daczko, N. R., 2017, Mass transfer in the lower crust: Evidence for incipient melt assisted flow along grain boundaries in the deep arc granulites of Fiordland, New Zealand: *Geochemistry, Geophysics, Geosystems*, v. 17, no. 9, p. 3733-3753.
- Stuart, C. A., Meek, U., Daczko, N. R., Piazzolo, S., and Huang, J. X., 2018a, Chemical Signatures of Melt–Rock Interaction in the Root of a Magmatic Arc: *Journal of Petrology*, v. 59, no. 2, p. 321-340.
- Stuart, C. A., Piazzolo, S., and Daczko, N. R., 2018b, The recognition of former melt flux through high-strain zones: *Journal of Metamorphic Geology*, v. 36, no. 8, p. 1049-1069.
- Taylor, S. R., and McLennan, S. M., 1986, *The continental crust: its composition and evolution*, Volume 42, p. 196-197.
- Tulloch, A. J., Ireland, T. R., Kimbrough, D. L., Griffin, W. L., Ramezani, J., Tulloch, A. J., and mq-iris:0000043076, 2011, Autochthonous inheritance of zircon through Cretaceous partial melting of Carboniferous plutons : the Arthur River Complex, Fiordland, New Zealand, Springer.
- Vavra, G., Schmid, R., and Gebauer, D., 1999, Internal morphology, habit and U-Th-Pb microanalysis of amphibolite-to-granulite facies zircons: geochronology of the Ivrea Zone (Southern Alps): *Contributions to Mineralogy and Petrology*, v. 134, no. 4, p. 380-404.
- Vernon, R. H., 2011, Microstructures of melt-bearing regional metamorphic rocks, Origin and Evolution of Precambrian High-Grade Gneiss Terranes, with Special Emphasis on the Limpopo Complex of Southern Africa, p. 1-11.
- Victoria Elliott, 2015. Zircon growth and modification during deep melt flux through a magmatic arc. [M.Research thesis]: Sydney, Australia: Macquarie University
- Weinberg, R. F., 1996, Ascent mechanism of felsic magmas: news and views: *Transactions of the Royal Society of Edinburgh: Earth Sciences*, v. 87, no. 04, p. 541.
- Weinberg, R. F., and Hasalová, P., 2015, Water-fluxed melting of the continental crust: A review: *Lithos*, v. 212-215, p. 158-188.
- Winter, J. D., 2014, *Principles of igneous and metamorphic petrology* / John D. Winter, Harlow Pearson Education.
- Wu, Y., and Zheng, Y., 2004, Genesis of zircon and its constraints on interpretation of U-Pb age: *Chinese Science Bulletin*, v. 49, no. 15, p. 1554-1569.
- Zhu, W., Gaetani, G. A., Fusseis, F., Montési, L. G. J., and De Carlo, F., 2011, Microtomography of Partially Molten Rocks: Three-Dimensional Melt Distribution in Mantle Peridotite: *Science*, v. 332, no. 6025, p. 88-91.